Available online at www.sciencedirect.com
SCIENCE DIRECT®
Remote Sensing of Environment 89 (2004) 326–350
Remote Sensing of Environment
www.elsevier.com/locate/rse

An evaluation of MODIS and SeaWiFS bio-optical algorithms in the Baltic Sea

Miroslaw Darecki[a,*], Dariusz Stramski[b]

[a] Institute of Oceanology, Polish Academy of Sciences, Powstancow Warszawy 55, 81-712 Sopot, Poland
[b] Marine Physical Laboratory, Scripps Institution of Oceanography, University of California at San Diego, La Jolla, CA 92093-0238, USA

Received 29 April 2003; received in revised form 15 October 2003; accepted 23 October 2003

Abstract

An extensive bio-optical data set from field measurements was used to evaluate the performance of standard Moderate Resolution Imaging Spectroradiometer (MODIS) and Sea-viewing Wide Field-of-view Sensor (SeaWiFS) ocean color (in-water) algorithms in the Baltic Sea, which represents an example of optically complex Case 2 waters with high concentration of colored dissolved organic matter (CDOM). The data set includes coincident measurements of radiometric quantities, chlorophyll *a* concentration (Chl *a*), and absorption coefficient of CDOM, which were taken on 25 cruises between 1993 and 2001. The data cover a wide range of variability with Chl *a* in surface waters from about 0.3 to 100 mg m^{-3}. All the MODIS pigment algorithms examined as well as the SeaWiFS OC4v4 algorithm showed a systematic and large overestimation in chlorophyll retrievals. The mean systematic and random errors based on our entire data set exceeded 150% or even 200% in some cases, making these standard algorithms inadequate for pigment determinations in the Baltic. Although new parameterization of the standard pigment algorithms based on our field measurements in the Baltic resulted in a significant reduction of errors, the overall performance of such regionally tuned algorithms remained unsatisfactory. For example, the mean normalized bias (MNB) for the regionally tuned MODIS chlor_a_2 algorithm was reduced to 26% (from over 200% for the standard algorithm), but the root mean square (RMS) error was still large (>100%). The MODIS K_490 algorithm for estimating the diffuse attenuation coefficient of downwelling irradiance showed the best performance among all the algorithms examined. With the new coefficients based on our field data, the regional version of this algorithm showed an acceptable level of errors, MNB = 4% and RMS = 30%. In addition to the apparent problems of the standard in-water bio-optical algorithms, we found that the atmospheric correction currently in use for MODIS and SeaWiFS imagery usually fails to retrieve upwelling radiances emerging from the Baltic Sea. The match-up comparisons of the coincident in situ and satellite determinations of normalized water-leaving radiances showed generally poor agreement, especially in the blue spectral region. It appears that new approaches for ocean color algorithms are required in the Baltic Sea.

Keywords: Ocean color; Remote sensing; Baltic Sea; Chlorophyll; MODIS; SeaWiFS

1. Introduction

Ocean color is a unique property because it can be measured from space to provide synoptic global information on subsurface oceanographic parameters that represent the upper ocean from the surface to a few tens of meters depth. The ocean color is the spectrum of radiation from sun and sky in the visible region, which emerges from below the sea surface after being scattered upward at subsurface depths. This spectrum of water-leaving radiance is influenced by concentrations and optical properties of various organic and inorganic constituents of seawater. To date, most of the quantitative applications of ocean color remote sensing have focused on the determinations of abundance and distribution of phytoplankton chlorophyll in the world's oceans. Such determinations are based essentially on changes of ocean color from blue to green as the chlorophyll concentration increases. These capabilities were first demonstrated by aircraft measurements (Clarke, Ewing, & Lorenzen, 1970), and the NASA's proof-of-concept satellite mission Coastal Zone Color Scanner (CZCS) (Gordon, Clark, Mueller & Hovis, 1980; Hovis et al., 1980).

Building upon the CZCS heritage (Evans & Gordon, 1994), significant efforts have been made in the recent past

* Corresponding author. Tel.: +48-58-5517281; fax: +48-58-5512130.
E-mail addresses: darecki@iopan.gda.pl (M. Darecki), stramski@mpl.ucsd.edu (D. Stramski).

0034-4257/$ - see front matter © 2003 Elsevier Inc. All rights reserved.
doi:10.1016/j.rse.2003.10.012

to develop ocean color satellite missions with improved spectral and radiometric performance, spatial and temporal coverage, and quality of data products (Morel, 1998). In the United States, these efforts resulted in the Sea-viewing Wide Field-of-view Sensor (SeaWiFS) (Hooker & McClain, 2000) that was launched on the OrbView-2 spacecraft in August 1997, and the Moderate Resolution Imaging Spectroradiometers (MODIS) (Esaias et al., 1998) that were launched on the NASA Earth Observing System (EOS) satellites Terra and Aqua, in December 1999 and May 2002, respectively. With these missions, we entered a new era of ocean color remote sensing that is expected to provide a highly consistent time series of near-synoptic and global data for many years to come.

Atmospheric correction and in-water bio-optical algorithms are the key components in processing satellite ocean color data. To date, ocean color algorithm development has focused largely on ocean waters for which simplifying assumptions about the optical properties can be made. Specifically, it has been assumed that over 90% of surface waters in the world oceans can be classified as Case 1 waters, in which phytoplankton and covarying material of biological origin are principal water constituents responsible for variations in ocean optical properties (Gordon & Morel, 1983; Morel & Prieur, 1977). In Case 1 waters, substances other than phytoplankton are either optically insignificant or correlated with phytoplankton. Although this idea oversimplifies the reality to some extent (Siegel & Michaels, 1996; Stramski & Tegowski, 2001; Terrill, Melville, & Stramski, 2001), it provided an essential stimulus for the advancement of ocean color remote sensing in recent decades. The Case 1 water assumptions imply that the ocean optical properties can be modeled as a function of chlorophyll concentration alone, which has led to algorithms for retrieving phytoplankton pigments from remotely sensed ocean color. The current satellite operational algorithms for retrieval of pigments and other bio-optical properties have been empirically derived from field data collected mainly in ocean waters that are assumed to be Case 1 (e.g., O'Reilly et al., 1998, 2000).

According to a bipartite classification scheme, optically complex waters that cannot be classified as Case 1 are designated as Case 2 waters. Typically, Case 2 waters include coastal and inland water bodies where agents other than phytoplankton such as suspended inorganic particles and/or dissolved organic matter (and perhaps even a bottom reflectance) make a significant contribution to the optical properties (e.g., Bukata, Jerome, Kondratyev, & Pozdnyakov, 1995; Sathyendranath, 2000). In Case 2 waters, these agents vary independently of phytoplankton and each other. The consequences of such complexity are that single-variable optical models based on chlorophyll are generally inadequate. In particular, the standard algorithms in use today for chlorophyll retrieval from satellite data of ocean color usually break down in Case 2 waters (e.g., Sathyendranath, 2000). It is well recognized that Case 2 waters require new algorithms based on new approaches for dealing with both atmospheric correction and retrievals of ocean bio-optical properties from water-leaving radiance (Sathyendranath, 2000). The prospects of better remote sensing of Case 2 waters is now improving with technological advances in ocean color sensors and scientific efforts underway to gain an in-depth understanding of optics in Case 2 waters. However, before future achievements in these areas are applied to remote sensing, routine processing of global satellite data from sensors such as MODIS will probably continue to be executed indiscriminately for all waters of the world's oceans with standard algorithms designed primarily for Case 1 waters. Therefore, it is useful to develop an understanding of limitations and to quantify errors of current standard algorithms in various Case 2 waters, especially as no specific algorithms exist that would allow masking of regions where Case 1 algorithms may not hold.

The Baltic Sea is of particular interest with respect to such an analysis. This is an intracontinental shallow marine environment under strong influence of human activities and terrestrial material, which has obvious economic, social, and ecological significance. Case 2 waters in the Baltic are often dominated by colored dissolved organic matter (CDOM). Large discharge from rivers, limited exchange with marine waters of the North Sea, and a relatively shallow sea floor significantly influence the optical properties of the Baltic. In addition to the high concentration of CDOM that exerts a profound effect on the absorption properties (Højerslev & Aas, 2001; Kowalczuk, 1999; Kowalczuk & Darecki, 1998), the Baltic waters are also rich in nutrients. This increases the primary production, which sometimes results in unusually high chlorophyll concentrations, even close to 100 mg m^{-3}. It has been demonstrated that the common blue-to-green ratios of ocean reflectance do not provide the best algorithm for chlorophyll retrieval in the Baltic (Darecki, Weeks, Sagan, Kowalczuk, & Kaczmarek, 2003). Thus, a comprehensive analysis of the performance of standard algorithms that are based on the blue-green bands in the Baltic should be beneficial for the current use of remote sensing and future efforts on algorithm development.

The main purpose of this work is to test the performance of several standard bio-optical MODIS algorithms and one standard SeaWiFS chlorophyll algorithm in the Baltic Sea using a large data set from field measurements taken over a period of 9 years between 1993 and 2001. As inputs to the algorithms, we used the spectral remote-sensing reflectance, $R_{rs}(\lambda)$, and the spectral normalized water-leaving radiance, $L_{wn}(\lambda)$, determined from our in-water radiometric measurements of spectral downwelling irradiance, $E_d(z,\lambda)$, and spectral upwelling radiance, $L_u(z,\lambda)$, and above-water measurements of downwelling irradiance, $E_s(\lambda)$ (where λ is light wavelength in a vacuum). The data products retrieved from the algorithms are compared with in situ determinations of the chlorophyll *a* concentration, diffuse attenuation coefficient for downwelling irradiance at $\lambda = 490$ nm, $K_d(490)$, and the absorption coefficient by CDOM at 400 nm, $a_{CDOM}(400)$. We also assembled a match-up database that allowed direct comparisons of in situ determinations of $L_{wn}(\lambda)$ with satellite-derived $L_{wn}(\lambda)$ from MODIS and SeaWiFS sensors in the Baltic as well as match-up comparisons of in situ determinations chlorophyll *a* concentration, $K_d(490)$ and $a_{CDOM}(400)$ with satellite-derived values of these quantities.

2. In situ data and methods

The validation of five standard bio-optical MODIS algorithms and one SeaWiFS algorithm (see Appendix A) was carried out with field data collected on 25 cruises in the years 1993–2001 (Table 1). The data were collected mainly in the southern part of the Baltic Sea (Fig. 1) under various environmental conditions in different seasons of the year. The spatial coverage includes very turbid waters in the Gulf of Gdansk and Pomeranian Bay; coastal waters along the Polish coast; and less turbid waters further away from the coast and in the central Baltic. The seasonal coverage includes (i) winter data with relatively low chlorophyll concentrations and stable absorption background from CDOM (this season is characterized by strong mixing processes driven by wind and vertical thermohaline circulation, and limited riverine discharge); (ii) spring data with high freshwater runoff and strong phytoplankton blooms; and (iii) late summer and autumn data with occasional phytoplankton blooms.

The above-described division of our data set is often shown on the graphs to demonstrate the presence or absence of spatial and/or seasonal dependency of the analyzed relationships. For the total number of 932 underwater radiometric measurements taken during 9 years between 1993 and 2001, 707 cases were accompanied by measurements of chlorophyll *a* concentration in surface waters.

2.1. Radiometric measurements

The spectral remote-sensing reflectance and normalized water-leaving radiance were calculated from underwater measurements of the vertical profiles of spectral upwelling radiance, $L_u(\lambda,z)$, and spectral downwelling irradiance, $E_d(z,\lambda)$, made with a spectroradiometer MER2040 (Biospherical Instruments). The instrument was equipped with 10 spectral channels (412, 443, 490, 510, 550, 590, 625, 665, 683 and 710 nm) for both $L_u(z,\lambda)$ and $E_d(z,\lambda)$ measurements. The radiometer was calibrated every year or every 2 years at the manufacturer's laboratory. During 8 years of use, no major drift of calibration constants was observed. The dark current readings were controlled and appropriate corrections were applied at all times. Additionally, several intercalibrations with other instruments were performed on some cruises, which confirmed the stability of the instrument calibration. Our radiometric measurements were consistent with the protocol developed for the SeaWiFS project (Mueller & Austin, 1995), including the correction for instrument

Table 1
The list of cruises in the Baltic Sea and the number of optical and pigment measurements made on each cruise

Cruise	Date	$R_{rs}(\lambda)$ and $K_d(\lambda)$	Chl(spectrophotometric)	Chl *a*(HPLC)	a_{CDOM}
1	September 6–October 1, 1993	48	32	–	16
2	April 11–April 17, 1994	33	32	–	18
3	May 7–May 15, 1994	28	–	–	21
4	August 17–August 25, 1994	43	32	–	22
5	September 23–September 27, 1994	26	22	–	18
6	September 7–September 14, 1995	40	21	–	12
7	October 13–October 20, 1995	19	9	–	–
8	March 8–March 17, 1996	31	29	–	29
9	May 18–May 26, 1996	33	30	–	30
10	September 13–September 22, 1996	29	27	–	19
11	March 13–March 23, 1997	54	30	–	51
12	April 17–April 20, 1997	18	18	–	13
13	May 19–May 26, 1997	50	21	–	35
14	August 30–September 8, 1997	59	52	–	55
15	February 25–March 4, 1998	24	26	–	26
16	May 5–May 12, 1998	31	32	14	29
17	September 18–September 25, 1998	32	26	19	20
18	April 20–April 28, 1999	43	42	37	42
19	February 16–March 8, 2000	52	46	46	46
20	May 8–May 14, 2000	31	27	27	19
21	September 21–September 30, 2000	52	49	49	48
22	February 17–February 25, 2001	27	26	26	25
23	May 5–May 16, 2001	72	51	52	49
24	September 6–September 19, 2001	40	30	30	30
25	October 11–October 21, 2001	19	–	–	–

These numbers are given for the remote-sensing reflectance, $R_{rs}(\lambda)$, the attenuation coefficient of downwelling irradiance, $K_d(\lambda)$, the chlorophyll determinations with spectrophotometric method, Chl(spectrophotometric), and HPLC method, Chl *a*(HPLC), and the absorption coefficient by CDOM, a_{CDOM}.

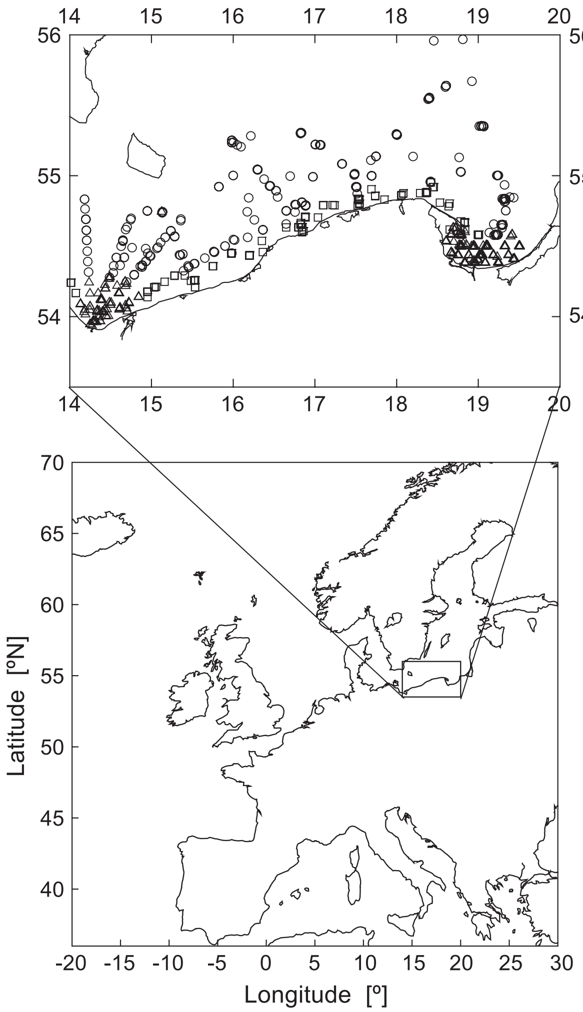

Fig. 1. Location of stations in the Baltic Sea where bio-optical measurements were made in the years from 1993 to 2001. The triangles represent stations in very turbid waters in the Gulf of Gdansk and Pomeranian Bay, the squares are the stations in coastal waters of the southern Baltic along the Polish coast, and the circles are the stations in less turbid waters further away from the Polish coast and in the central Baltic.

self-shading (Gordon & Ding, 1992; Zibordi & Ferrari, 1995). The MER 2040 spectroradiometer was deployed using a 6–8-m-long boom or crane on the sunny side of the ship's stern, away from the ship shadow. All measurements were performed on the R/V *Oceania*, which is a relatively small vessel (50 m long, 3.5 m draught). The MER2040 measurements were accompanied by the above-water measurements of spectral downwelling irradiance, $E_s(\lambda)$, with a sensor mounted on the ship deck. All profiles of $E_d(z,\lambda)$ and $L_u(z,\lambda)$ and above-water measurements of $E_s(\lambda)$ were graphed and carefully examined as a quality check. All measurements in which significant and rapid changes in the ambient light occurred during vertical profiling, and any peculiar spectra were eliminated from the analysis.

We examined the effects of MER2040 self-shading on the upwelling radiance just below the sea surface, $L_u(z=0^-,\lambda)$, by calculating the parameter $\xi=[L_u(z=0^-,\lambda) - L_{u,M}(z=0^-,\lambda)]/L_u(z=0^-,\lambda)$, where L_u is the corrected radiance and $L_{u,M}$ is the measured radiance uncorrected for self-shading. These calculations indicated that the correction is important for the Baltic waters, especially in the blue and red spectral regions where the radiance attenuation is relatively strong. For the blue and green wavebands of particular interest to this study, we found that ξ was, on average, 0.21 at 443 nm (with a standard deviation $\sigma_\xi=0.15$), 0.14 at 490 nm ($\sigma_\xi=0.12$), and 0.1 at 550 nm ($\sigma_\xi=0.09$). These values indicate that the corrected $L_u(z=0^-,\lambda)$ was higher typically by about 10% in the green to over 20% in the blue compared to the uncorrected measured radiances. Because the standard empirical algorithms for processing MODIS and SeaWiFS data are based on the blue-to-green band ratios, it is instructive to note that the self-shading correction resulted, on average, in a 13% increase of $L_u(z=0^-,443)/L_u(z=0^-,550)$ and a 4% increase of $L_u(z=0^-,490)/L_u(z=0^-,550)$ for our data set from the Baltic. These numbers are low enough to suggest that even if our self-shading correction was inaccurate, the possible inaccuracies would not be sufficient to have a significant qualitative impact on our major conclusions presented in the following sections. In particular, a large bias of the standard bio-optical algorithms in the Baltic, which is demonstrated and discussed below, is very unlikely to be caused by inaccuracies in our self-shading correction.

The remote-sensing reflectance, $R_{rs}(\lambda)$, was calculated as the ratio of the upwelling radiance just above the water surface, $L_w(\lambda)$, to downwelling irradiance measured above the water, $E_s(\lambda)$. The water-leaving radiance $L_w(\lambda)$ was obtained from the upwelling radiance estimated just below the water surface, $L_u(z=0^-,\lambda)$, and propagated through the water–air interface using a factor of 0.544, so the formula for $R_{rs}(\lambda)$ is

$$R_{rs}(\lambda) = 0.544\frac{L_u(z=0^-,\lambda)}{E_s(\lambda)} \tag{1}$$

Then, the normalized water-leaving radiance $L_{wn}(\lambda)$ was calculated from

$$L_{wn}(\lambda) = F_o(\lambda)R_{rs}(\lambda) \tag{2a}$$

where $F_o(\lambda)$ is the mean extraterrestrial solar irradiance at a given spectral band. For the three blue-green spectral bands centered at 443, 488, and 551 nm, which are of primary interest to this study, the F_o values are (in mW cm^{-2} µm^{-1})

$$F_o(443) = 189.45,\ F_o(488) = 193.66,\ F_o(551) = 185.33 \tag{2b}$$

To obtain $L_u(z=0^-,\lambda)$, the measurements of the upwelling radiance, $L_u(z,\lambda)$, were extrapolated from a depth of 1.5–2 m to the surface using the attenuation coefficient for upwelling radiance, $K_{Lu}(z,\lambda)$. $K_{Lu}(z,\lambda)$ was calculated as the local slope of $\ln[L_u(z,\lambda)]$ measured within a depth interval spanning a few meters within the surface layer. The thickness of this depth interval depended on the extent to which the surface layer was homogeneous. Typically it was about 3 m. The noisy data due to the effects of surface waves observed near the surface were excluded from the analysis. In a similar way, the diffuse attenuation coefficient for downwelling irradiance, $K_d(z,\lambda)$, was calculated from the $E_d(z,\lambda)$ profiles.

2.2. Chlorophyll a measurements

On all cruises, the chlorophyll *a* concentration was determined using the spectrophotometric method (HELCOM, 1988). The samples of surface water were filtered under low pressure (less than 0.5 atm) using Whatman glass-fiber filters (GF/F 47 mm in diameter). The particulate matter retained on the filters was extracted for 24 h in 96% ethanol. The absorbance of the extract was measured on a Specord M40 (before 1998) and Unicam UV4-100 (since 1998) spectrophotometer. The following equation was used to convert the absorbance at 665 nm to chlorophyll *a* concentration:

$$\mathrm{Chl[mg\ \ m^{-3}]} = 10^3(D_{665} - D_{750})v83^{-1}r^{-1}V^{-1} \qquad (3)$$

where D_{665} is the absorbance at 665 nm (after correction for blank ethanol), D_{750} the absorbance at 750 nm (after correction for blank ethanol), v the volume of ethanol (ml), r the cell (cuvette) pathlength (cm), V the volume of filtered seawater (l), and 83 (l g^{-1} cm^{-1}) is the chlorophyll *a*-specific absorption coefficient in ethanol (Schotz, 1962). Here, we use the symbol Chl (rather than Chl *a*) to indicate that this spectrophotometric method does not yield an estimate of pure chlorophyll *a* concentration. In this method, the value of Chl can (and generally does) include contributions from other pigments, especially phaeopigments.

Since 1998, additional samples were taken for the analysis of pigments by high-performance liquid chromatography (HPLC). In total, we analyzed 300 samples with HPLC, which provided the estimates of the concentration of chlorophyll *a*. We note that our HPLC estimates of chlorophyll *a* do not include contributions from its derivatives (chlorophyllide *a*, chlorophyll *a* allomers and epimers). Although HPLC methods are currently considered to be more accurate than spectrophotometric and fluorometric methods, we decided to use the spectrophotometric data as this allowed us to work with a much more extensive data set, namely, 707 spectrophotometric measurements. However, for comparative purposes, in the analysis of the performance of the pigment algorithms, we do provide results for the subset of about 300 HPLC measurements (Table 2).

Both methods for measuring chlorophyll concentration (spectrophotometric and HPLC) were compared and a good correlation between the measured chlorophyll values was found for the investigated Baltic waters (Fig. 2a). The regression between the HPLC and spectrophotometric data with a slope of nearly 1 was independent of season and pigment concentration:

$$\log[\mathrm{Chl}\ a(\mathrm{HPLC})] = 1.0003\log[\mathrm{Chl(spectrophotometric)}] - 0.1947 \qquad (4)$$

where the squared correlation coefficient between the log-transformed data is 0.92, and the number of observations $n = 300$. Assuming the slope of 1, this equation can be rewritten as

$$\mathrm{Chl(spectrophotometric)} = 1.57\mathrm{Chl}\ a(\mathrm{HPLC}) \qquad (5)$$

The acidification of the samples was also tested with the spectrophotometric technique, and the results are compared to the HPLC method (Fig. 2b). The average offset that was significant in Fig. 2a (the spectrophotometric values were lower, on average, by about 35% than the HPLC values) is now only 5%. This indicates that phaeopigments are largely responsible for the systematic differ-

Table 2
Summary of the error analysis for the standard MODIS and SeaWiFS pigment algorithms

Parameter	Field data	MNB (%)	RMS (%)	log_bias	log_rms	n
CZCS_pigm	Chl(spectrophotometric)	1730	20800	0.43	0.47	707
	Chl(spectrophotometric; Limited data set $[(y_{alg} - y_{obs})/y_{obs}] \times 100 < 1000\%$	188	194	0.36	0.32	664
chlor_MODIS	Chl *a*(spectrophotometric)	540	4500	0.43	0.38	707
	Chl *a*(spectrophotometric); Limited data set $[(y_{alg} - y_{obs})/y_{obs}] \times 100 < 1000\%$	187	174	0.38	0.27	671
	Chl *a*(HPLC)	1098	8292	0.42	0.49	298
chlor_a_2	Chl *a*(spectrophotometric)	236	309	0.42	0.29	707
	Chl *a*(spectrophotometric); Limited data set $[(y_{alg} - y_{obs})/y_{obs}] \times 100 < 1000\%$	209	179	0.41	0.27	699
	Chl *a*(HPLC)	246	321	0.40	0.36	298
chlor_a_3	Chl *a*(spectrophotometric)	375	764	0.53	0.32	707
	Chl *a*(spectrophotometric); Limited data set $[(y_{alg} - y_{obs})/y_{obs}] \times 100 < 1000\%$	272	225	0.49	0.28	672
	Chl *a*(HPLC)	431	984	0.53	0.40	298
OC4v4	Chl *a*(spectrophotometric)	177	234	0.34	0.29	707
	Chl *a*(spectrophotometric); Limited data set $[(y_{alg} - y_{obs})/y_{obs}] \times 100 < 1000\%$	159	155	0.33	0.28	700
	Chl *a*(HPLC)	183	231	0.32	0.37	299

ence between our spectrophotometric and HPLC chlorophyll data in Fig. 2a because phaeopigments have significant contribution to our spectrophotometric estimates of Chl. The scatter of data points in Fig. 2b is, however, relatively large as the normalized root mean square error (see Eq. (8b)) is 52% compared to 33% in Fig. 2a. This suggests that the spectrophotometric measurements of samples upon acidification do not provide robust estimates of pure chlorophyll *a*. Therefore, for the validation of the MODIS and SeaWiFS algorithms for retrieving chlorophyll *a* concentration, our Chl estimates from the spectrophotometric measurements (before acidification) were all multiplied by 0.64 according to Eq. (5) in order to obtain the 'HPLC-equivalent' estimates of pure chlorophyll *a* indicated as Chl *a*(spectrophotometric):

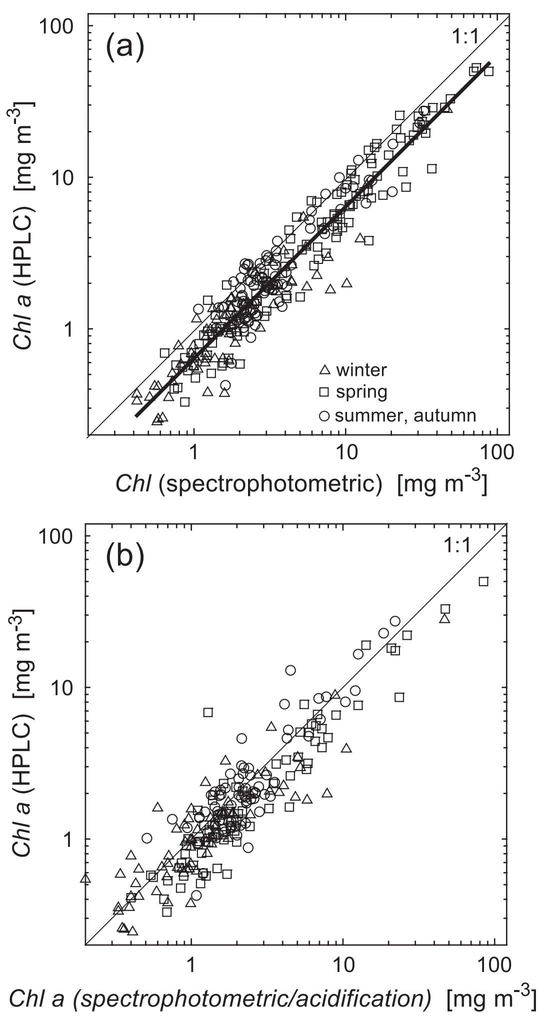

Fig. 2. Comparisons of the HPLC-measured chlorophyll *a* concentrations, Chl *a*(HPLC), with chlorophyll concentrations from spectrophotometric method: (a) spectrophotometric chlorophyll estimates, Chl(spectrophotometric), represent direct spectrophotometric determinations on untreated samples (before acidification); (b) spectrophotometric chlorophyll estimates, Chl *a*(spectrophotometric/acidification), represent spectrophotometric determinations on samples after acidification. The thin solid lines represent the one-to-one perfect agreement between the compared quantities. The thick solid line in panel (a) is the best fit linear regression.

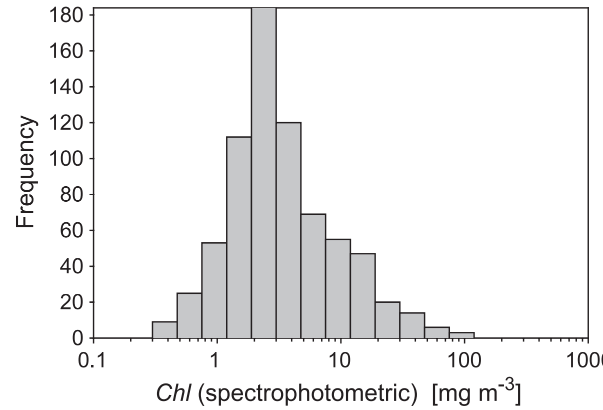

Fig. 3. Frequency distribution of the chlorophyll concentration data obtained from spectrophotometric measurements.

$$\mathrm{Chl}\ a(\mathrm{spectrophotometric}) \approx \mathrm{Chl}\ a(\mathrm{HPLC}) = 0.64\mathrm{Chl}(\mathrm{spectrophotometric}) \quad (6)$$

For the validation of one algorithm (CZCS_pigm algorithm) that provides a pigment data product which is the sum of chlorophyll *a* and phaeopigments, we used the values of Chl directly from our spectrophotometric measurements (before acidification). The histogram distribution of Chl based on the whole data set is presented in Fig. 3, which shows a wide range of concentration from about 0.3 to about 100 mg m^{-3}. The Chl values between 2 and 3 mg m^{-3} occur most frequently.

We note that a relationship similar to our Eq. (5) was presented earlier between the data representing the sum of the concentrations of chlorophyll *a* and phaeopigments (Chl *a* + Phaeo) and the data representing the chlorophyll *a* concentration from the SeaBASS Historical Pigment Database (O'Reilly et al., 1998):

$$\mathrm{Chl}\ a + \mathrm{Phaeo} = 1.34(\mathrm{Chl}\ a)^{0.983} \quad (7)$$

Most of the SeaBASS data were from the Atlantic and Pacific waters off the US coast. For those data, the multiplicative factor in Eq. (7) is lower than the analogous factor in Eq. (5) for our Baltic Sea data.

3. Evaluation of the MODIS and SeaWiFS bio-optical algorithms

We will now evaluate the performance of five MODIS algorithms and one SeaWiFS algorithm in the Baltic using our field data of remote-sensing reflectance and normalized water-leaving radiance as inputs to the algorithms. The evaluation process is based on a comparison of the algorithm-derived values of the pigment concentration,

$a_{\mathrm{CDOM}}(400)$ and $K_{\mathrm{d}}(490)$, with field observations of these bio-optical quantities. The algorithms examined in this study are described in detail in Appendix A.

3.1. Evaluation criteria

For the purpose of the evaluation of the algorithm performance, the mean normalized bias (MNB) (systematic error) as well as the normalized root mean square (RMS) error (random error) were calculated. These errors (in percent) are defined as follows:

$$\mathrm{MNB} = \mathrm{mean}[(y_{\mathrm{alg}} - y_{\mathrm{obs}})/y_{\mathrm{obs}}]100 \tag{8a}$$

$$\mathrm{RMS} = \mathrm{stdev}[(y_{\mathrm{alg}} - y_{\mathrm{obs}})/y_{\mathrm{obs}}]100 \tag{8b}$$

where y_{alg} is the chlorophyll concentration or other bio-optical product estimated from the algorithm, y_{obs} is the observed value of the bio-optical quantity (measured in situ), and mean and stdev indicate the calculations of the mean and standard deviation values, respectively:

$$\mathrm{mean}(\chi) = \bar{\chi} = \frac{1}{n}\sum_{i=1}^{n}\chi_i$$

$$\mathrm{stdev}(\chi) = \left[\frac{1}{n-1}\sum_{i=1}^{n}(\chi_i - \bar{\chi})^2\right]^{1/2}$$

where χ is the variable of interest [i.e., the relative errors defined as $(y_{\mathrm{alg}} - y_{\mathrm{obs}})/y_{\mathrm{obs}}$ in Eqs. (8a) and (8b)] and n the number of observations. We also used the statistics based on the root mean square of the logarithm of the ratio of algorithm-derived to measured values, which were recently used in the ocean color literature (e.g., O'Reilly et al., 1998). Such statistics can provide a good measure of data scatter for lognormally distributed variables, which is often observed for chlorophyll data sets. These types of error were calculated from the following equations:

$$\mathrm{log\_bias} = \mathrm{mean}[\log(y_{\mathrm{alg}}/y_{\mathrm{obs}})] \tag{9a}$$

$$\mathrm{log\_rms} = \mathrm{stdev}[\log(y_{\mathrm{alg}}/y_{\mathrm{obs}})] \tag{9b}$$

3.2. Evaluation results

Comparisons of the measured and algorithm-derived estimates of chlorophyll products from the MODIS and SeaWiFS algorithms are presented in Figs. 4–8. The measured values of Chl obtained directly from the spectrophotometric method were used in the evaluation of the MODIS CZCS_pigm algorithm (Fig. 4). For the evaluation of the three other MODIS pigment algorithms, referred to as chlor_MODIS, chlor_a_2, and chlor_a_3, as well as the SeaWiFS OC4v4 algorithm, we used the spectrophotometric measurements of chlorophyll corrected according to Eq. (6), which provided the HPLC-equivalent chlorophyll a concentration, Chl a

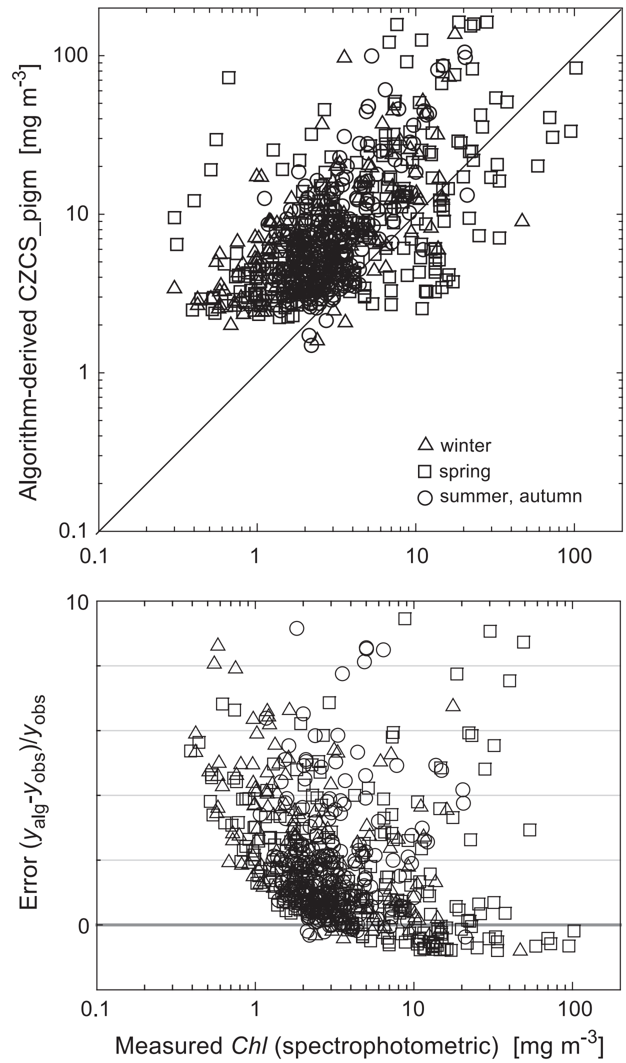

Fig. 4. Comparisons between the chlorophyll concentration derived from the MODIS CZCS_pigm algorithm and field spectrophotometric determinations on surface water samples. Top panel: algorithm-derived estimates vs. measured chlorophyll concentration. The line represents one-to-one perfect agreement. Bottom panel: the relative error in algorithm-derived estimates vs. measured chlorophyll concentration. On both graphs, the different symbols correspond to data collected in different seasons of the year as indicated. The same scheme of symbols is applied to data presented in (Figs. 5, 6, 8–10, and 12–15).

(Figs. 5–8). We also tested these pigment algorithms by comparing the algorithm-derived Chl a with Chl a obtained directly from HPLC. Similar comparisons of the algorithm-derived data products and measurements are shown in Figs. 9 and 10 for $a_{\mathrm{CDOM}}(400)$ and $K_{\mathrm{d}}(490)$, respectively. The error calculations based on Eqs. (8a), (8b), (9a), and (9b) are summarized in Tables 2 and 3.

In general, the MODIS and SeaWiFS pigment algorithms significantly overestimated chlorophyll concentration in the whole range of concentrations (Figs. 4–8 and Table 2). Only a small fraction of the examined data, 11% for CZCS_pigm, 8% for chlor_MODIS, 6% for chlor_a_2, 4% for chlor_a_3, and 8% for OC4v4, shows some underestimation in the

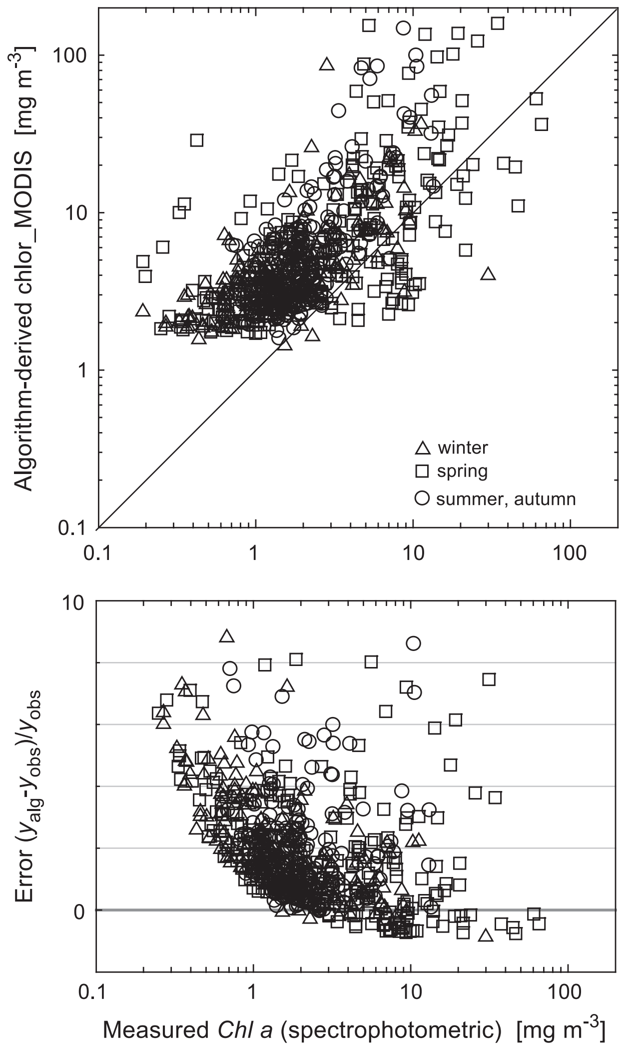

Fig. 5. Comparisons between the chlorophyll *a* concentration derived from the chlor_MODIS algorithm and field spectrophotometric determinations on surface water samples. Top panel: algorithm-derived estimates vs. measured chlorophyll concentration. The line represents one-to-one perfect agreement. Bottom panel: the relative error in algorithm-derived estimates vs. measured chlorophyll concentration.

algorithm-derived pigment concentration. This underestimation is observed only at relatively high concentrations >2–5 mg m^{-3}. The MODIS CZCS_pigm algorithm gives in many cases very high overestimation of Chl (Fig. 4). This overestimation is often unrealistically high, which is also seen in Fig. 11 where the frequency distributions of the errors for the entire data set of 707 measurements are displayed. In 43 out of 707 cases, the CZCS-pigm estimates were more than 10 times higher than the measured values of Chl. When such data with $[(y_{\mathrm{alg}} - y_{\mathrm{obs}})/y_{\mathrm{obs}}] \times 100 > 1000\%$ are omitted in the statistical analysis, the mean errors are considerably smaller but still very large (see the error values for the limited data set in Table 2). An overall poor performance is also noticed for the chlor_MODIS algorithm (Fig. 5). In 36 out of 707 cases, the chlor_MODIS estimates of chlorophyll *a* concentration were more than 10 times higher than the measured values of Chl *a*. If we ignore these outlying data, the mean systematic and random errors still remain high (Table 2). In addition, Table 2 shows that if we use the measured Chl *a* obtained directly from HPLC instead of the spectrophotometrically based Chl *a* (Eq. (6)) in the evaluation of chlor_MODIS algorithm, no improvement of the algorithm performance is observed. This conclusion applies also to the chlor_a_2, chlor_a_3, and OC4v4 algorithms that are discussed below (see Table 2).

The CZCS_pigm and chlor_MODIS algorithms were designed primarily for Case 1 waters, where optically significant constituents of seawater are assumed to covary with chlorophyll concentration (Gordon & Morel, 1983; Morel & Prieur, 1977). The Baltic waters do not satisfy this assumption and can be classified as Case 2 waters, so the overall poor performance of Case 1 water algorithms in the Baltic is not surprising (Darecki et al., 2003). The next two

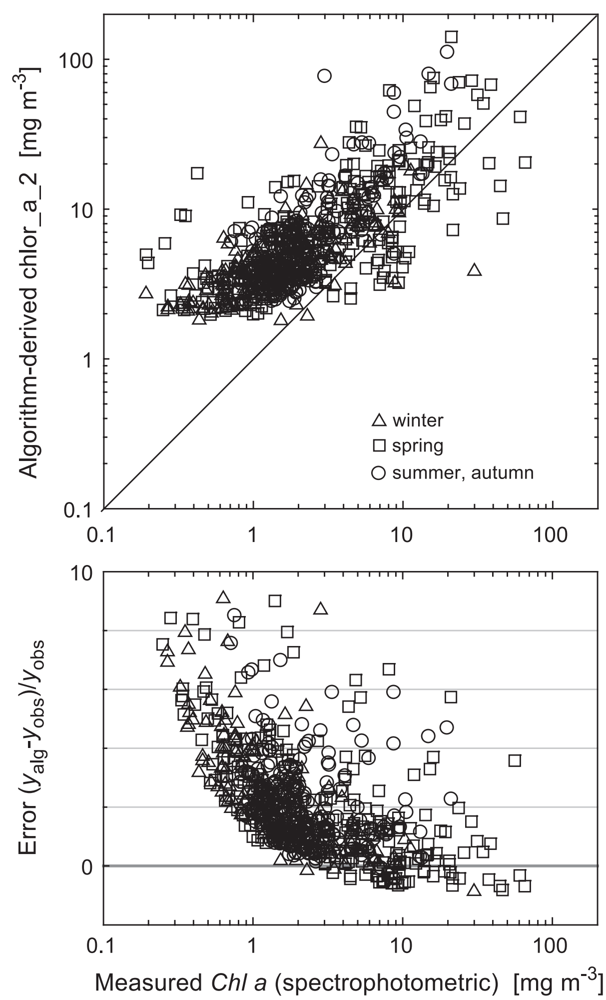

Fig. 6. Comparisons between the chlorophyll *a* concentration derived from the MODIS chlor_a_2 algorithm and field spectrophotometric determinations on surface water samples. Top panel: Algorithm-derived estimates vs. measured chlorophyll concentration. The line represents one-to-one perfect agreement. Bottom panel: The relative error in algorithm-derived estimates vs. measured chlorophyll concentration.

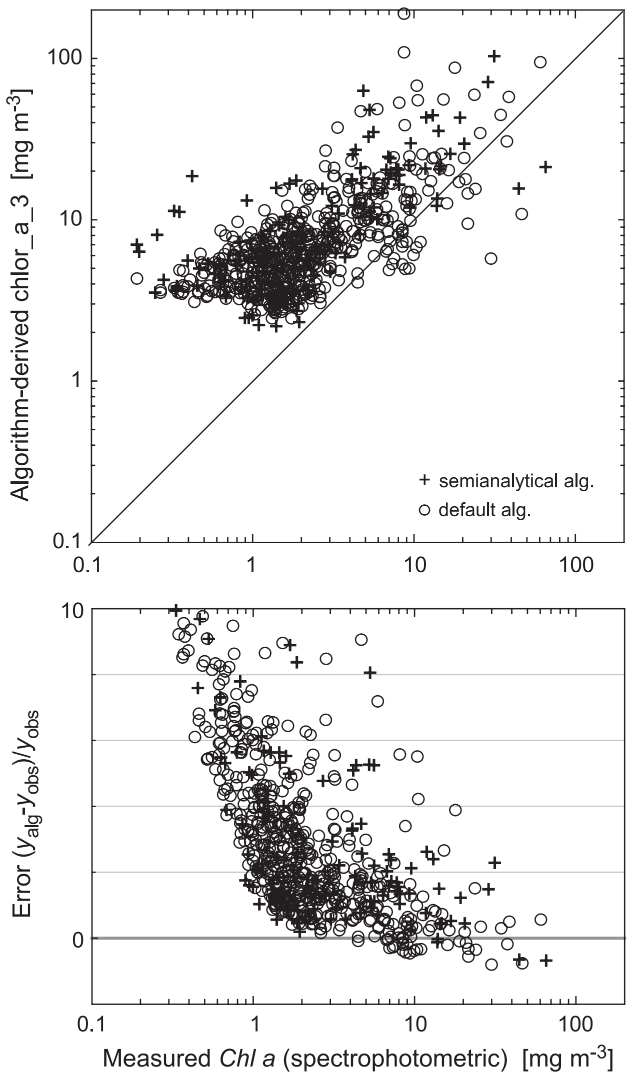

Fig. 7. Comparisons between the chlorophyll *a* concentration derived from the MODIS chlor_a_3 algorithm and field spectrophotometric determinations on surface water samples. Top panel: algorithm-derived estimates vs. measured chlorophyll concentration. The line represents one-to-one perfect agreement. Bottom panel: the relative error in algorithm-derived estimates vs. measured chlorophyll concentration. On the graph, the different symbols correspond to data derived from semianalytical or default mode of the algorithm.

MODIS algorithms, chlor_a_2 and chlor_a_3, have been designed to retrieve the chlorophyll *a* concentration with a purpose of achieving a better performance in Case 2 waters without compromising the performance in Case 1 waters. Thus, we expect that these algorithms may perform better in the Baltic than chlor_MODIS and CZCS_pigm. The chlor_a_2 algorithm (also referred to as OC3M, see O'Reilly et al., 2000) is a MODIS version of the SeaWiFS OC4 algorithm. The development of chlor_a_2 algorithm was based on the same data set as OC4v4, and it uses a similar fourth-order polynomial equation. The difference is that chlor_a_2 uses three MODIS spectral bands and OC4v4 uses four SeaWiFS bands. The chlor_a_2 algorithm still exhibits a significant overestimation of Chl *a* in the Baltic (Fig. 6), but the values of mean errors for the entire data set of 707 measurements are considerably lower than those for CZCS_pigm and chlor_MODIS (Table 2). Only in 8 out of 707 cases, the chlor_a_2 estimates were 10 times higher than the measured Chl *a*. Importantly, however, if these outliers are omitted from the error analysis, the resulting mean errors for such a limited data set are not necessarily smaller than the corresponding errors of the CZCS_pigm and chlor_MODIS algorithms.

The systematic and random errors for the MODIS chlor_a_3 algorithm are larger than those for the chlor_a_2 algorithm (Fig. 7 and Table 2). In 35 out of 707 cases, the chlor_a_3 estimates were more than 10 times higher than the measured values of Chl *a*. After excluding these outliers, the mean systematic and random errors remain the highest

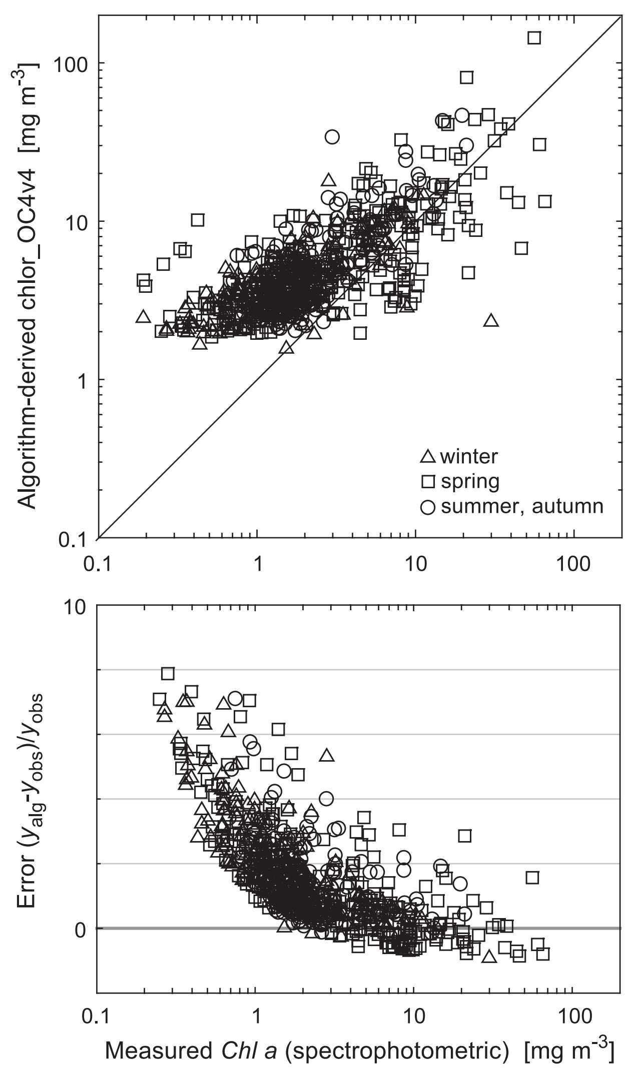

Fig. 8. Comparisons between the chlorophyll *a* concentration derived from the SeaWiFS OC4v4 algorithm and field spectrophotometric determinations on surface water samples. Top panel: algorithm-derived estimates vs. measured chlorophyll concentration. The line represents one-to-one perfect agreement. Bottom panel: the relative error in algorithm-derived estimates vs. measured chlorophyll concentration.

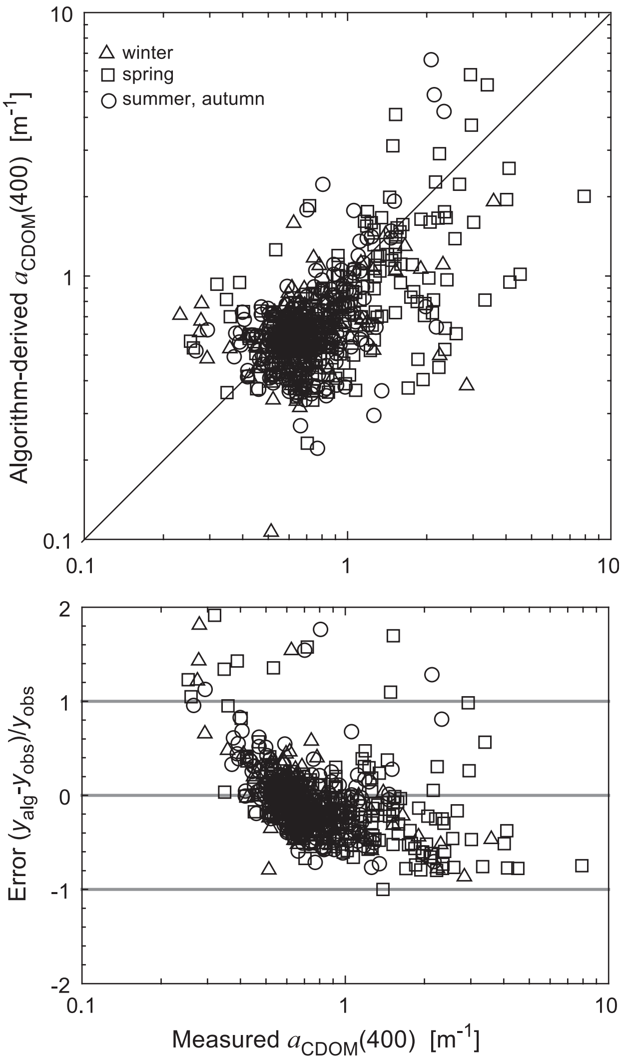

Fig. 9. Comparisons between the CDOM absorption coefficient at 400 nm derived from MODIS algorithm and field measurements on surface water samples. Top panel: algorithm-derived estimates vs. measured values of $a_{\mathrm{CDOM}}(400)$. The line represents one-to-one perfect agreement. Bottom panel: the relative error in algorithm-derived estimates vs. measured $a_{\mathrm{CDOM}}(400)$.

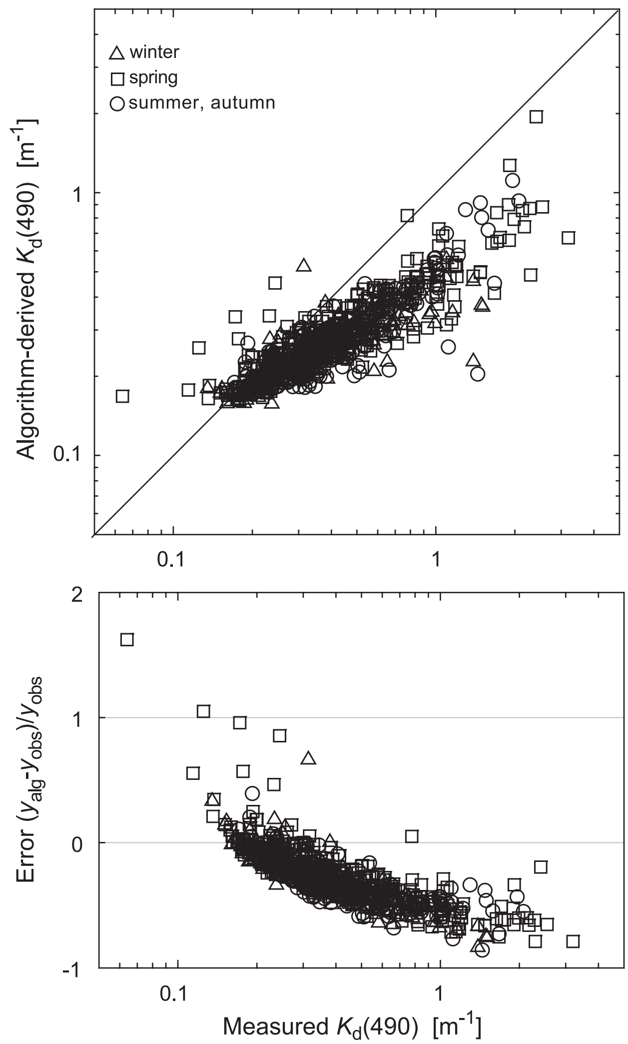

Fig. 10. Comparisons between the diffuse attenuation coefficient for downwelling irradiance at 490 nm derived from MODIS algorithm and in situ measurements. Top panel: algorithm-derived estimates vs. measured values of $K_d(490)$. The line represents one-to-one perfect agreement. Bottom panel: the relative error in algorithm-derived estimates vs. measured $K_d(490)$.

among the algorithms compared. This is a significant and unexpected result because it was anticipated that the chlor_a_3 algorithm may perform better in Case 2 waters such as the Baltic Sea. The chlor_a_3 algorithm is distinctive among the pigment algorithms analyzed in this study because it is based on a semianalytical, bio-optical model of remote-sensing reflectance, $R_{\mathrm{rs}}(\lambda)$ (Carder, Chen, Lee, & Hawes, 1999; Carder, Chen, Lee, Hawes, & Cannizzaro, 2003). All other algorithms, CZCS_pigm, chlor_MODIS, chlor_a_2, and OC4v4, are purely empirical in that they apply simple regressions between the field determinations of pigment concentration and the spectral ratios of ocean reflectance or normalized water-leaving radiance.

The semianalytical $R_{\mathrm{rs}}(\lambda)$ model of the chlor_a_3 algorithm has two free variables, the absorption coefficient of phytoplankton at 675 nm, $a_{\Phi}(675)$ and the absorption coefficient of CDOM at 400 nm, $a_{\mathrm{CDOM}}(400)$. The $R_{\mathrm{rs}}(\lambda)$ model also includes several empirically derived parameters which control the spectral shapes of the optical constituents of the model. Using the $R_{\mathrm{rs}}(\lambda)$ values as input, this model is inverted to yield $a_{\Phi}(675)$ and $a_{\mathrm{CDOM}}(400)$. If the value of $a_{\Phi}(675)$ is inside a predetermined range, the chlorophyll a concentration is calculated directly from the empirical

Table 3
Summary of the error analysis for the standard MODIS algorithms for CDOM absorption and diffuse attenuation of irradiance

Parameter	MNB (%)	RMS (%)	log_bias	log_rms	n
absorp_coeff_gelb [$a_{\mathrm{CDOM}}(400)$]	− 7	40	− 0.07	0.18	656
K_490 [$K_d(490)$]	− 27	22	− 0.16	0.13	845

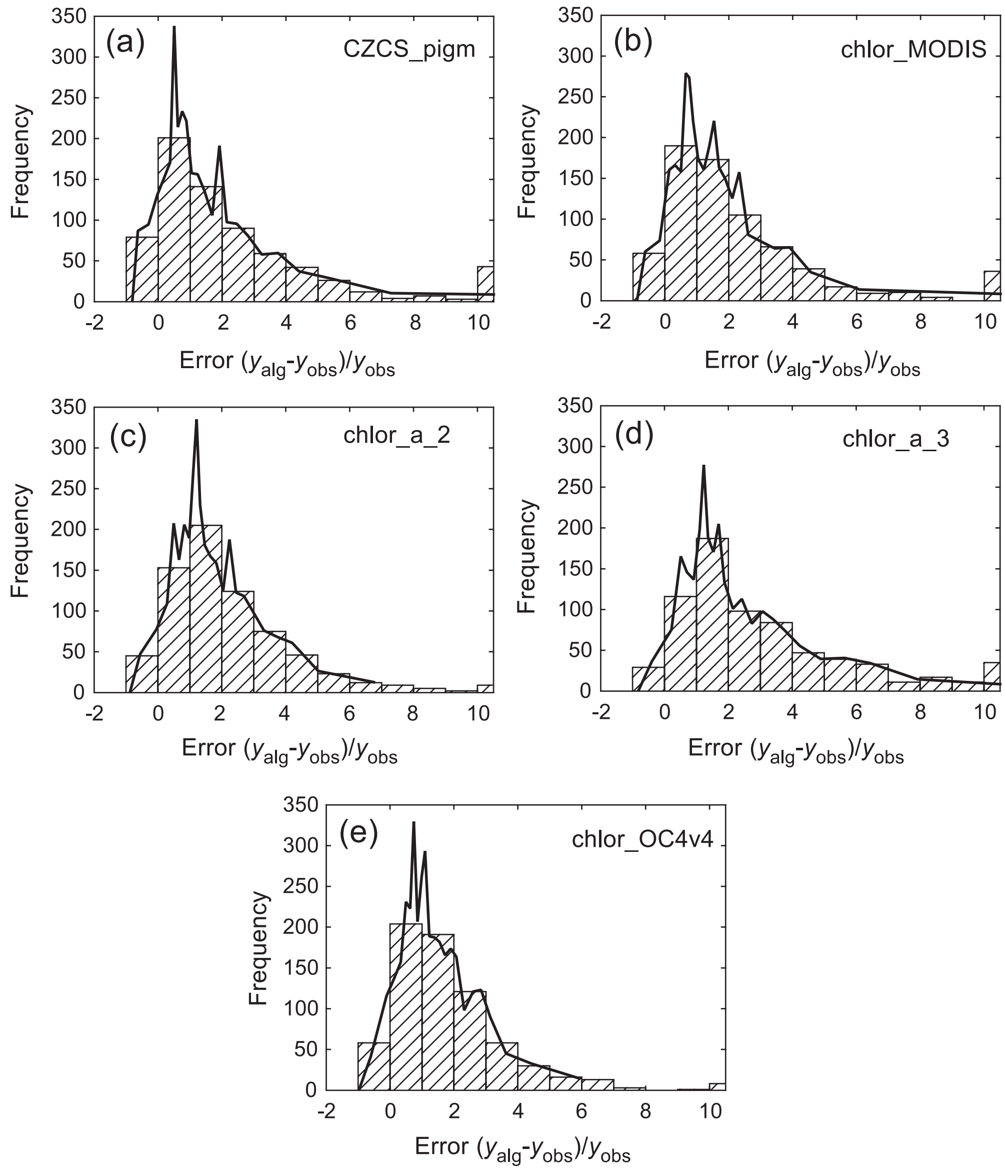

Fig. 11. Density function of the probability distribution (solid line) and histogram of the relative error of the algorithm-derived chlorophyll concentrations for each pigment algorithm as indicated in panels.

relationship between $a_{\Phi}(675)$ and Chl *a*. This type of algorithm operation is referred to as the "semianalytical" case. Otherwise, when the value of $a_{\Phi}(675)$ is outside a predetermined range, the default empirical algorithm based on a two-band reflectance ratio, $R_{rs}(488)/R_{rs}(551)$, is used to calculate Chl *a*. This mode of algorithm operation is called the "empirical" or "default" case. For the default case, the retrievals of $a_{\Phi}(675)$ and $a_{CDOM}(400)$ are also based solely on the empirical relationships involving the blue-to-green ratios of R_{rs} (see Appendix A).

When applied to our Baltic data, only for 142 out of 707 measurements considered in Fig. 7 and Table 2, the algorithm-derived Chl *a* values were calculated from the full semianalytical mode of algorithm operation. The remaining portion of chlorophyll determinations (i.e., 80%) was made with the default empirical algorithm. Our evaluation of chlor_a_3 suggests that this algorithm, like other MODIS algorithms, is not suitable for the Baltic waters. Because most chlor_a_3 calculations were made with the default empirical algorithm, the empirical parameters of this algorithm appear to be inappropriate for the Baltic. The present parameterization of the semianalytical model of the chlor_a_3 algorithm also appears to be inappropriate for the Baltic, as indicated by the scatter of semianalytically derived data points in Fig. 7.

In addition to the four MODIS pigment algorithms, we evaluated the OC4v4 algorithm currently used for global SeaWiFS processing (Fig. 8 and Table 2). In terms of the mean statistical errors, the OC4v4 algorithm performs better than the MODIS algorithms, and this also explains why the chlor_a_2 (OC3M) algorithm is the best among all MODIS algorithms. We recall that the chlor_a_2 and OC4 algorithms are both based on the same empirical SeaBAM data set (O'Reilly et al., 2000) that is significantly larger than the data set used for developing other MODIS algorithms. In our analysis, the mean systematic error MNB for OC4v4 is the smallest among the algorithms considered, and we observed only seven extreme data outliers with $[(y_{alg} - y_{obs})/y_{obs}] \times 100 > 1000\%$. The MNB error for OC4v4 is, however, still very large (159% for the limited data set of 700 observations). This makes this algorithm, just like MODIS algorithms discussed above, unacceptable for applications in the Baltic Sea.

It is important to comment on the question of why the pigment algorithms examined in our study consistently show a tendency for large overestimation of the pigment concentration in the Baltic. The empirical pigment algorithms including the default chlor_a_3 algorithm are all based on the blue-to-green spectral ratios of normalized water-leaving radiance or remote-sensing reflectance. In the Baltic, such ratios are significantly reduced compared to typical ocean waters because of high absorption by CDOM in the Baltic (e.g., Højerslev & Aas, 2001; Kowalczuk, 1999). Most empirical data used in the development of the standard MODIS and SeaWiFS pigment algorithms were collected in ocean waters with a smaller contribution of CDOM than in the Baltic. This is certainly a major cause for the frequent overestimation observed in the algorithm-derived pigment values in the Baltic waters. This overestimation is clearly seen in the highly skewed frequency distribution of error for each algorithm in Fig. 11.

Because of the significant optical role of CDOM in the Baltic, it is of particular interest to examine the capability of the MODIS semianalytical algorithm (Carder et al., 1999) to retrieve the CDOM absorption coefficient at 400 nm. Importantly, just like in the case of the chlor_a_3 pigment data product, retrievals of $a_{CDOM}(400)$ were mostly accomplished with the default empirical algorithm (see Appendix A) rather than the full semianalytical model. Specifically, the default algorithm was used in 488 out of 656 cases considered in Fig. 9 and Table 3, and the semianalytical derivation of $a_{CDOM}(400)$ was used in the remaining 168 cases. Although a comparison between the algorithm-derived and measured values of $a_{CDOM}(400)$ shows a considerable scatter in the data points, the bias is not as large as that observed for the pigment algorithms (Fig. 9). The systematic error MNB for the retrieval of $a_{CDOM}(400)$ is relatively small (-7%), but the overall performance of the algorithm is degraded by a relatively large random error (RMS = 40%, see Table 3). This random error is, however, still significantly smaller compared to the pigment algorithms, for which all of the RMS values were well over 100% (Table 2). Although inaccuracies in the measurement of CDOM absorption may generally play some role in such algorithm evaluation (Mitchell et al., 2000; Mitchell, Kahru, Wieland, & Stramska, 2002), the CDOM absorption signal in the Baltic in the violet-blue spectral region is usually strong enough to ensure that this measurement is much more accurate than in typical open ocean waters (Kowalczuk, 1999).

The final MODIS algorithm that we evaluate here is the empirical K_490 algorithm for estimating the diffuse attenuation coefficient of downwelling irradiance at 490 nm, $K_d(490)$, from the blue-to-green band ratio of water-leaving radiance (Fig. 10 and Table 3). This algorithm performs better than other algorithms, especially in terms of significantly reduced scatter in the data points (Fig. 10, see also Table 3 where RMS = 22% for the entire data set of 845 observations). There is, however, a significant bias of underestimating $K_d(490)$ for the major part of the range of diffuse attenuation observed in the Baltic, that is for $K_d(490) > 0.2\ m^{-1}$.

4. Regional parameterization of bio-optical MODIS algorithms

The bio-optical MODIS algorithms with their present standard parameterization as well as the SeaWiFS OC4v4 algorithm discussed in the previous section are inappropriate for applications in the Baltic because large errors in the retrieved data products occur with high probability. The significant bias of the retrieved data products suggests, however, that it may be possible to improve the performance of these algorithms if we replace the standard parameter values (the various regression coefficients) with new values determined from our field measurements in the Baltic. We will now examine this approach for the three empirical MODIS pigment algorithms, CZCS_pigm, chlor_MODIS, and chlor_a_2, and the empirical MODIS K_490 algorithm. In this approach, while preserving a mathematical formula of the algorithms, we will use our field data from the Baltic to determine the best regional parameterization of the algorithms. In this regional parameterization, we will use the entire data set available to us, so we will not be able to evaluate the performance of our regional algorithms against an independent data set.

Fig. 12 (upper panel) shows our measurements of Chl vs. the band ratio of normalized water-leaving radiance at 443 and 551 nm, which is used in the MODIS CZCS_pigm algorithm for retrieving the concentration of chlorophyll *a* plus phaeopigments. This figure also shows how the standard CZCS_pigm algorithm compares to the best fit regression, which represents our new regional algorithm referred to as Baltic_CZCS_pigm. Whether or not the higher order terms associated with the L_{wn} ratio were included in our regression analysis, the goodness of fit was about the same. Therefore, we propose a simple first-order formula for the regional Baltic_CZCS_pigm algorithm (Table 4). Note that this regional algorithm has a greatly reduced bias compared with the standard version of the CZCS_pigm algorithm (Fig. 12, lower panel) although the mean systematic error is still

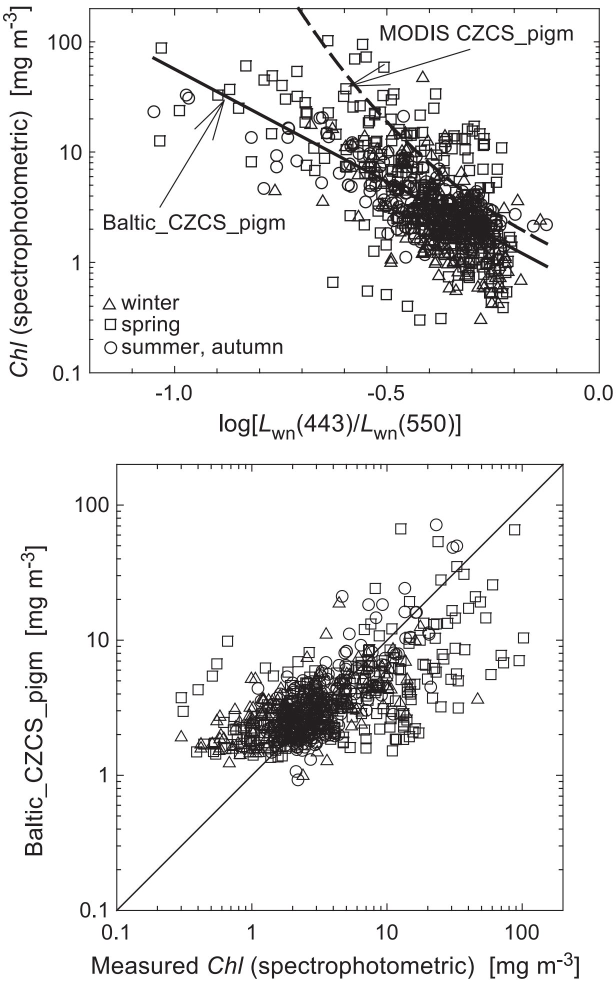

Fig. 12. Regional version of the MODIS CZCS_pigm algorithm for the Baltic Sea. Top panel: relationship between the surface chlorophyll concentration and the spectral band ratio of normalized water-leaving radiance based on our field measurements. The dashed line is the standard MODIS CZCS_pigm algorithm, and the solid line is the regional Baltic_CZCS_pigm algorithm based on the best fit to the data points. Bottom panel: estimates of chlorophyll concentration from the regional Baltic_CZCS_pigm algorithm vs. measured chlorophyll concentration. The line represents the perfect agreement.

significant (MNB = 32%, see Table 5). The random error for the Baltic_CZCS_pigm remains quite large (RMS = 130%, Table 5), but it is smaller than that for the standard CZCS_pigm algorithm. As mentioned above, we have no independent data to evaluate the regional algorithm, so we must bear in mind that the graphical presentation in the lower panel of Fig. 12 and the error analysis summarized in Table 5 use the same data as the algorithm development itself illustrated in the upper panel of Fig. 12.

Similar results and conclusions are found when developing the regional versions of the two MODIS algorithms for retrieving the chlorophyll *a* concentration, chlor_MODIS and chlor_a_2 (Figs. 13 and 14; Tables 4 and 5). Compared to the regional Baltic_CZCS_pigm algorithm, the regional Baltic_chlor_MODIS and Baltic_chlor_a_2 algorithms show further, albeit not large, reduction in the systematic and random errors. The Baltic_chlor_a_2 algorithm with MNB = 26% and RMS = 114% appears to be slightly better than the two other regional pigment algorithms (Table 5). This small but clear improvement from the Baltic_CZCS_pigm to Baltic_chlor_MODIS and Baltic_chlor_a_2 is likely related to the role played by the 443-nm band in these algorithms. All retrievals of Chl *a* with the Baltic_chlor_a_2 algorithm are made using the ratio $L_{wn}(488)/L_{wn}(551)$ because this ratio is always higher than $L_{wn}(443)/L_{wn}(551)$ in our Baltic data set. Thus, the 443-nm band plays no role in this case. In contrast, the 443-nm band is important in the application of the chlor_MODIS algorithm, which always uses the ratio $[L_{wn}(443)+L_{wn}(488)]/L_{wn}(551)$, and even more important for the CZCS_pigm algorithm that relies entirely on $L_{wn}(443)/L_{wn}(551)$. Because the CDOM content in the Baltic waters is typically high and poorly correlated with the pigment concentration, and because the CDOM absorption affects the 443-nm band to a greater extent than longer wavelengths, it is reasonable to expect that pigment retrievals can be better with algorithms that utilize longer wavelengths than 443 nm (Darecki et al., 2003; Kowalczuk & Darecki, 1998). Here, we have not addressed the regional parameterization for the chlor_a_3 algorithm because our results for the Baltic_chlor_a_2 can be considered as representative of those that would be obtained for chlor_a_3. This is because the Baltic_chlor_a_2 algorithm uses just the $L_{wn}(488)]/L_{wn}(551)$ ratio, and the chlor_a_3 algorithm operates in the Baltic predominantly in the empirical mode which involves the same ratio of L_{wn}.

Table 4
Regional versions of the MODIS algorithms for the Baltic Sea

Algorithm	Band ratio X	Formula
Baltic_CZCS_pigm	$X = \log[L_{wn}(443)/L_{wn}(551)]$	$10^{-0.2886-2.041X}$
Baltic_chlor_MODIS	$X = \log[L_{wn}(443)+L_{wn}(488)/L_{wn}(551)]$	$10^{0.4692-2.6802X}$
Baltic_chlor_a_2	$X = \log\{\max[L_{wn}(443)/L_{wn}(551), L_{wn}(488)/L_{wn}(551)]\}$	$10^{0.1520\ 3.0558X}$
Baltic_K_490	$X = \log[L_{wn}(488)/L_{wn}(551)]$	$10^{-0.685-2.056X}$

Table 5
Summary of the error analysis for the regional (Baltic) MODIS algorithms

Algorithm	Field data	MNB (%)	RMS (%)	log_bias	log_rms	n
Baltic_CZCS_pigm	Chl (spectrophotometric)	32	130	0	0.33	707
Baltic_chlor_MODIS	Chl *a* (spectrophotometric)	28	120	0	0.31	707
Baltic_chlor_a_2	Chl *a* (spectrophotometric)	26	114	0	0.29	707
Baltic_K_490	$K_d(490)$	4	30	0	0.12	845

The regional Baltic_K_490 algorithm shows the best performance among the regional MODIS algorithms developed in our study. The field data of $K_d(490)$ plotted vs. $L_{wn}(488)/L_{wn}(551)$ exhibit much less 'random' scatter (Fig. 15, upper panel) than the field data of pigment concentration vs. the band ratios of L_{wn} (Figs. 12–14, upper panels). The best fit to the $K_d(490)$ vs. $L_{wn}(488)/L_{wn}(551)$ data efficiently removes the bias that was present in the standard MODIS K_490 algorithm. As a result, the regional Baltic_K_490 algorithm (Table 4) is characterized by relatively small mean systematic and random error values. The MNB value is only 4% and RMS is 30%, which is well below the values for the pigment algorithms (Table 5). The good performance of the Baltic_K_490 algorithm has special significance because this capability is important not only for remote sensing of K_d itself, but also for the application of remote-sensing algorithms that can retrieve the inherent optical properties of water, such as the absorption and backscattering coefficients (e.g., Loisel & Stramski, 2000; Loisel et al., 2001).

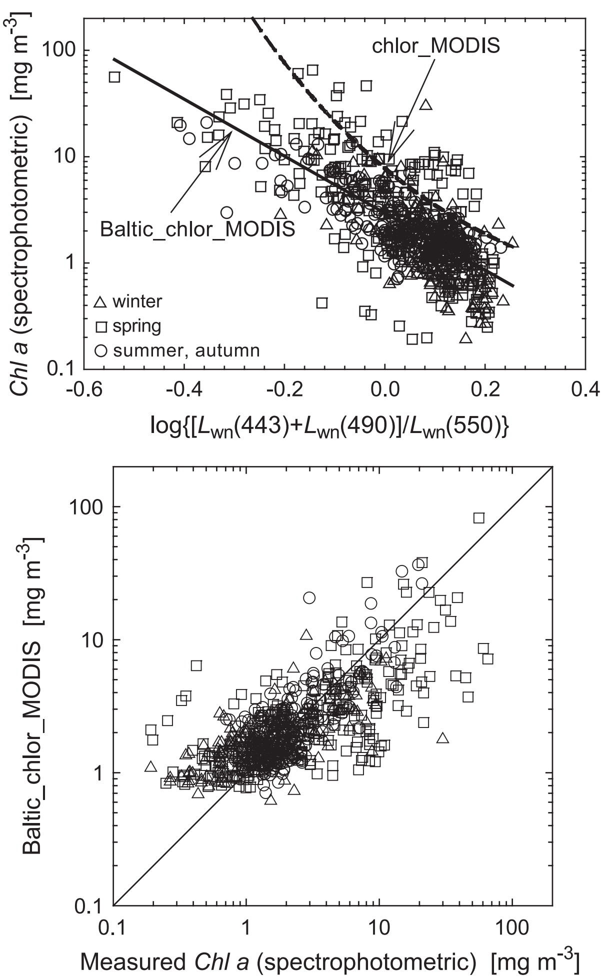

Fig. 13. Regional version of the chlor_MODIS algorithm for the Baltic Sea. Top panel: relationship between the surface chlorophyll concentration and the spectral band ratio of normalized water-leaving radiances based on field our measurements. The dashed line is the standard chlor_MODIS algorithm, and the solid line is the regional Baltic_chlor_MODIS algorithm based on the best fit to the data points. Bottom panel: estimates of chlorophyll concentration from the regional Baltic_chlor_MODIS algorithm vs. measured chlorophyll concentration. The line represents the one-to-one perfect agreement.

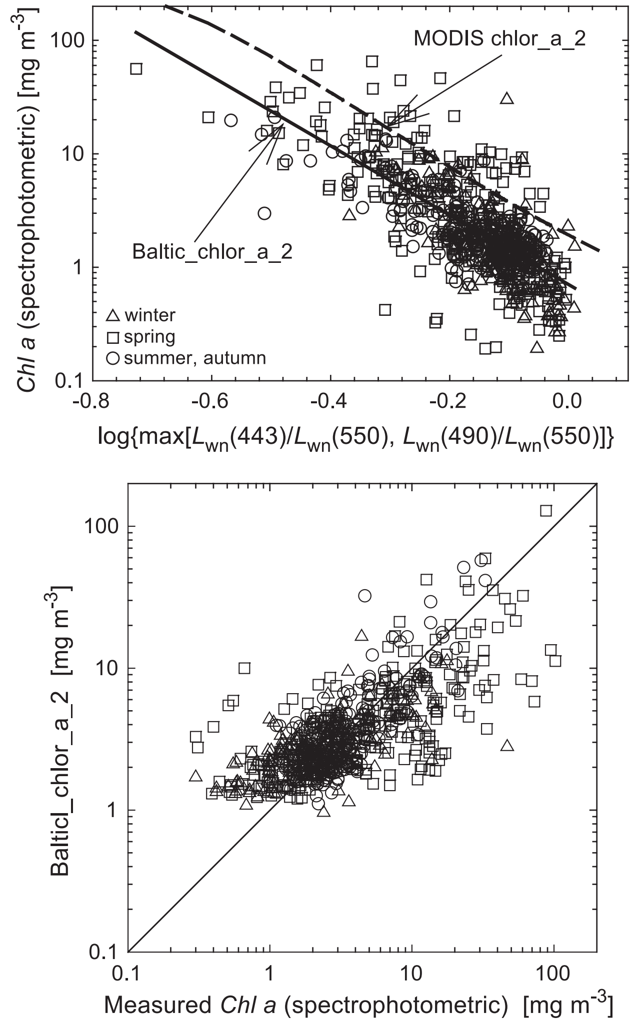

Fig. 14. Regional version of the MODIS chlor_a_2 algorithm for the Baltic Sea. Top panel: relationship between the surface chlorophyll concentration and the spectral band ratio of normalized water-leaving radiances based on our field measurements. The dashed line is the standard chlor_a_2 algorithm, and the solid line is the regional Baltic_chlor_a_2 algorithm based on the best fit to the data points. Bottom panel: estimates of chlorophyll concentration from the regional Baltic_chlor_a_2 algorithm vs. measured chlorophyll concentration. The line represents the one-to-one perfect agreement.

5. Comparison of satellite-derived data products with in situ measurements

Field measurements taken in the Baltic under cloud-free or partially cloud-free conditions (i.e., cloud-free skies above the area where the in situ measurements were carried out) in the years 2000 and 2001 were selected for match-up comparisons with MODIS data products obtained from

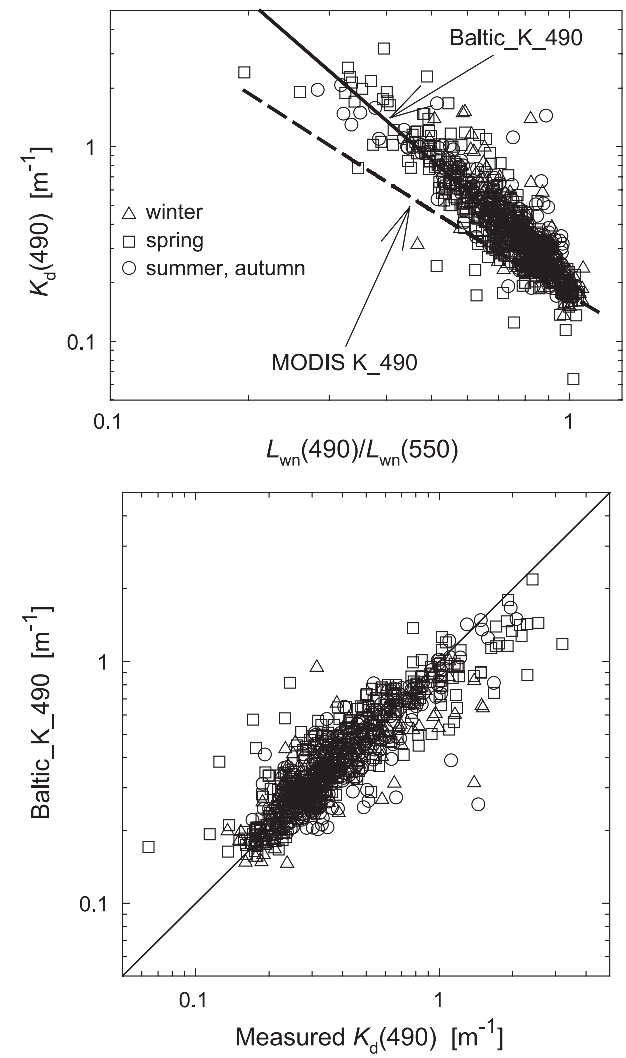

Fig. 15. Regional version of the MODIS K_490 algorithm for the Baltic Sea. Top panel: relationship between the diffuse attenuation coefficient for downwelling irradiance at 490 nm and the spectral band ratio of normalized water-leaving radiance based on our field measurements. The dashed line is the standard MODIS K_490 algorithm, and the solid line is the regional Baltic_K_490 algorithm based on the best fit to the data points. Bottom panel: estimates of diffuse attenuation coefficient from the regional Baltic_K_490 algorithm vs. measured attenuation coefficient. The line represents the one-to-one perfect agreement.

Terra satellite overpasses in the study region. Out of the total of 56 ship days at sea between September 2000 and October 2001, only 14 days qualified for the comparison with the satellite measurements. Seventeen MODIS granules that were processed for these days are listed in Table 6. The status of this processing is referred by NASA's MODIS/Terra project to as Terra MODIS Collection 4 v.4.2.2 reprocessing. The status of ocean color data products is referred to as provisional for satellite data collected before November 2000 and validated for data collected after November 2000. In our analysis, the provisional satellite data represent up to 20% of the total number of satellite data analyzed. The behavior of provisional data in the match-up comparisons is consistent with validated data.

Our match-up data set was divided according to the time shift between the satellite overpass and in situ measurements into three categories: (A) data with the time shift no greater than 1 h (triangles in Figs. 16–21); (B) data with the time shift of 1–4 h (squares); and (C) data with the time shift of 4–8 h (circles). Except for a few outlying data points, the data from category C are consistent with data from categories A and B.

The comparison of normalized water-leaving radiances, L_{wn}, obtained from the MODIS/Terra measurements and in situ measurements at five wavebands (412, 443, 488, 551, and 667 nm) shows generally poor agreement (Fig. 16). Apparently, this can be attributed primarily to the performance of the standard atmospheric correction procedure (Gordon, 1997; Gordon & Wang, 1994) in the Baltic Sea. Only the satellite radiometric data with the quality level 0 assigned to the satellite-derived L_{wn} are shown in Fig. 16. This quality level is assigned to the data pixels free from any problems that may occur in satellite data processing due to large solar zenith angles, clouds, sun glint contamination, shallow water, negative radiance retrievals, failed atmospheric correction, and/or questionable aerosol model. The MODIS L_{wn} data with quality level 0 are considered 'good' in contrast to 'questionable' or 'bad' data due to large zenith angle (quality level 1), cloud or sun glint contamination (quality level 2), and other reasons (quality level 3). The MODIS band centered at 531 nm is not included in Fig. 16 because of the lack of the corresponding spectral channel in our in situ spectroradiometer.

It is remarkable that the satellite-derived L_{wn} in the blue spectral bands (412, 443, and 488 nm) totally failed in this comparison with in situ determinations of L_{wn}. For example,

Table 6
MODIS granules used in the match-up analysis

Day of the year	MODIS granule
Year 2000	
266	2000266.1040
268	2000268.1025
271	2000271.1055
273	2000273.1045
Year 2001	
48	2001048.1010
128	2001128.1010
129	2001129.0915
129	2001129.1050
130	2001130.0955
131	2001131.1040
132	2001132.0945
132	2001132.1120
133	2001133.1025
134	2001134.0930
134	2001134.1110
135	2001135.1015
258	2001258.0950

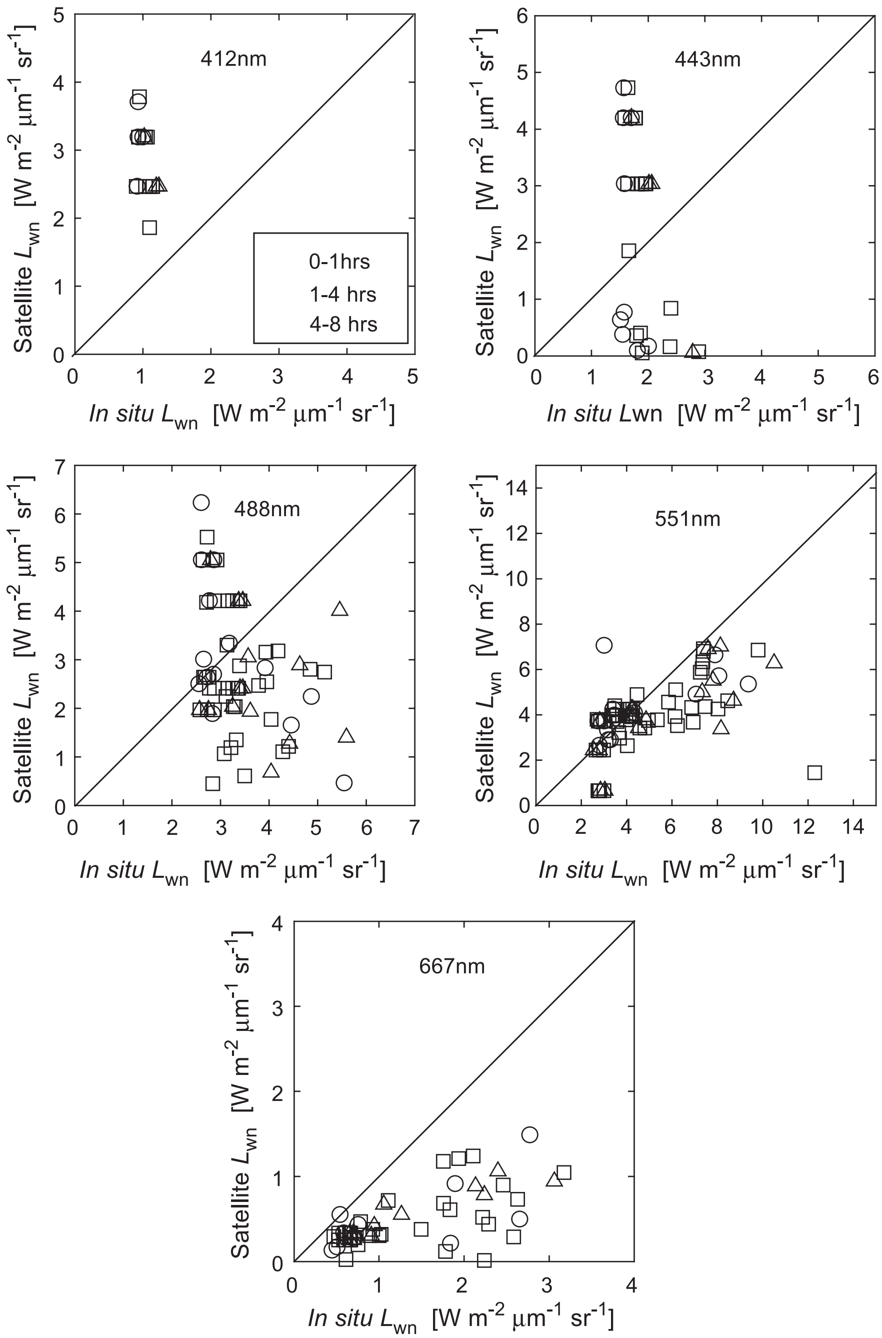

Fig. 16. Comparisons of match-up data of normalized water-leaving radiance measured in situ and derived from MODIS satellite imagery for spectral bands of 412, 443, 488, 551, and 667 nm. Only data with a quality level 0 for satellite-derived L_{wn} are presented. As indicated, the triangles represent match-up data with the time shift no greater than 1 h between the satellite overpass and in situ measurement, the squares correspond to the time shift of 1–4 h, and the circles to the time shift of 4–8 h. The line represents the one-to-one perfect agreement.

with the exception of a few data points, the satellite-derived values of L_{wn} at 488 nm are either significantly higher or significantly lower than the in situ L_{wn}, and there is no pattern of covariation between these two estimates. In the red band of 667 nm, the satellite-derived L_{wn} is consistently lower than the in situ L_{wn}, but the covariation is discernible. The data for the 551-nm band show the best agreement among the spectral channels compared in Fig. 16. There is a clear covariation between the satellite and in situ values of $L_{wn}(551)$, although the general trend shows a bias as the satellite determinations underestimate $L_{wn}(551)$ in comparison with in situ measurements at high values of $L_{wn}(551)$. The errors in the satellite-derived L_{wn} calculated from Eqs. (8a), (8b), (9a), and (9b) are summarized in Table 7. In these particular calculations, y_{alg} in the equations represent the satellite-derived L_{wn}.

Because the standard empirical bio-optical algorithms are based on the band ratio of water-leaving radiance or reflec-

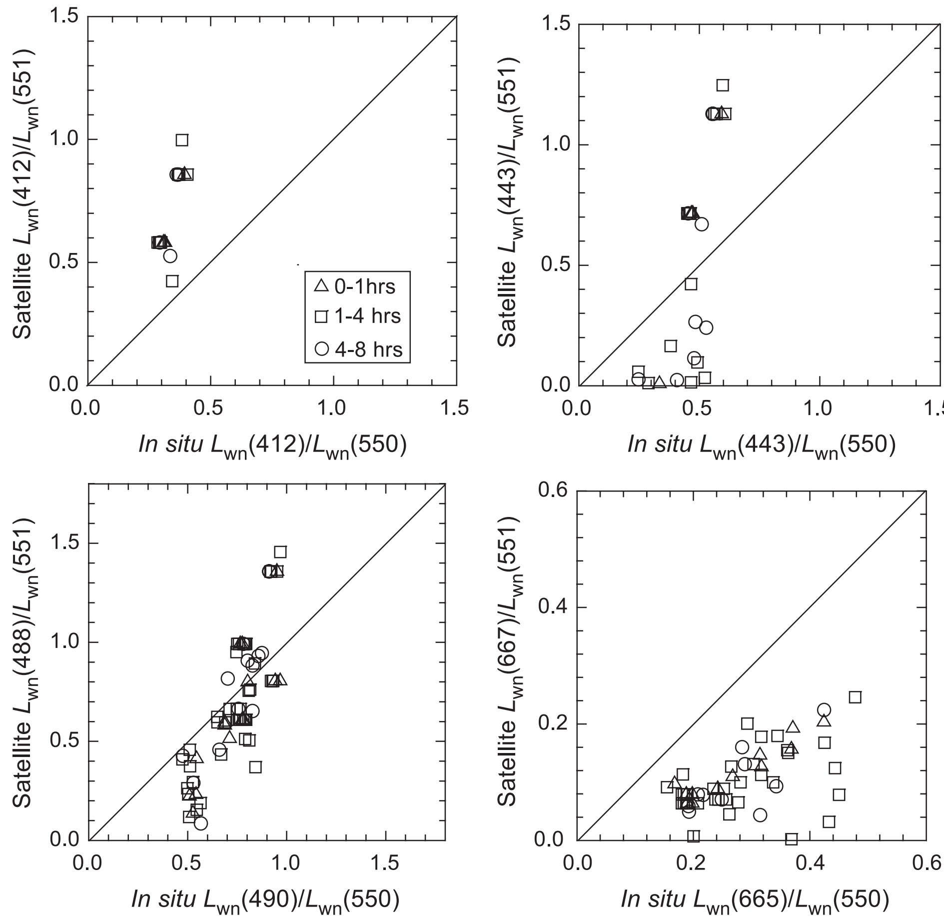

Fig. 17. As Fig. 16, but comparisons are shown for spectral band ratios of normalized water-leaving radiance.

tance, it is important to compare the satellite-derived and in situ ratios of L_{wn}. Hypothetically, if some systematic errors of the atmospheric correction affected the different spectral channels in a similar way, then the satellite-derived band ratios of L_{wn} could be subject to smaller errors than the magnitude of L_{wn} at single wavebands. However, our analysis does not support this hypothesis and shows generally poor agreement between the satellite and in situ determinations of the blue-to-green and red-to-green ratios of L_{wn} (Fig. 17). The satellite ratio $L_{wn}(488)/L_{wn}(551)$ appears to compare with its in situ counterpart better than the three other ratios shown in Fig. 17, but even in this case, the satellite determinations produce systematic underestimation compared with in situ measurements for low values of the band ratio. The general regularity of the satellite-derived vs. in situ-derived data points of L_{wn} band ratios, especially the 488:551-nm ratio, suggests that region-specific adjustments in the atmospheric correction procedure for the Baltic appear to be possible.

While several factors may be responsible for poor performance of the atmospheric correction procedure (Gordon, 1997; Siegel, Wang, Maritorena, & Robinson, 2000; Yan et al., 2002), it is of interest to evaluate first whether the discrepancies observed between the satellite-derived and in situ-derived L_{wn} values in the Baltic show any relation to water properties themselves. This evaluation is illustrated by plotting the ratio of satellite L_{wn} to in situ L_{wn} for five MODIS wavebands as a function of three water properties measured in situ, L_{wn}, $K_d(490)$, and Chl *a* (Fig. 18). Obviously, the ideal result would be to have all values of satellite-to-in situ ratio equal to 1. However, as seen in Fig. 18, the values close to 1 are scarce. In addition, these plots show that the L_{wn} ratio tends to decrease with increasing water turbidity which is reflected in an increase of in situ $K_d(490)$ and Chl *a* values. This tendency is particularly well pronounced at 551 nm, although it can also be observed at other wavelengths. Note that at 551 nm, good agreement between the satellite-derived and in situ measurements of L_{wn} (the ratio of these two values is close to 1) occurs in the relatively clear Baltic waters with the lowest values of $K_d(490)$ and chlorophyll *a* concentration of about 1 mg m^{-3} or less. For Chl *a* higher than 3 mg m^{-3}, the satellite-derived $L_{wn}(551)$ is consistently lower than the in situ $L_{wn}(550)$.

One possible source for an overcorrection of atmospheric effects and underestimation of L_{wn} is the violation of the black pixel assumption in the atmospheric correction procedure (e.g., Hu, Carder, & Muller-Karger, 2000; Ruddick, Ovidio, & Rijkeboer, 2000; Siegel et al., 2000). This assumption is that values of water-leaving radiance in the

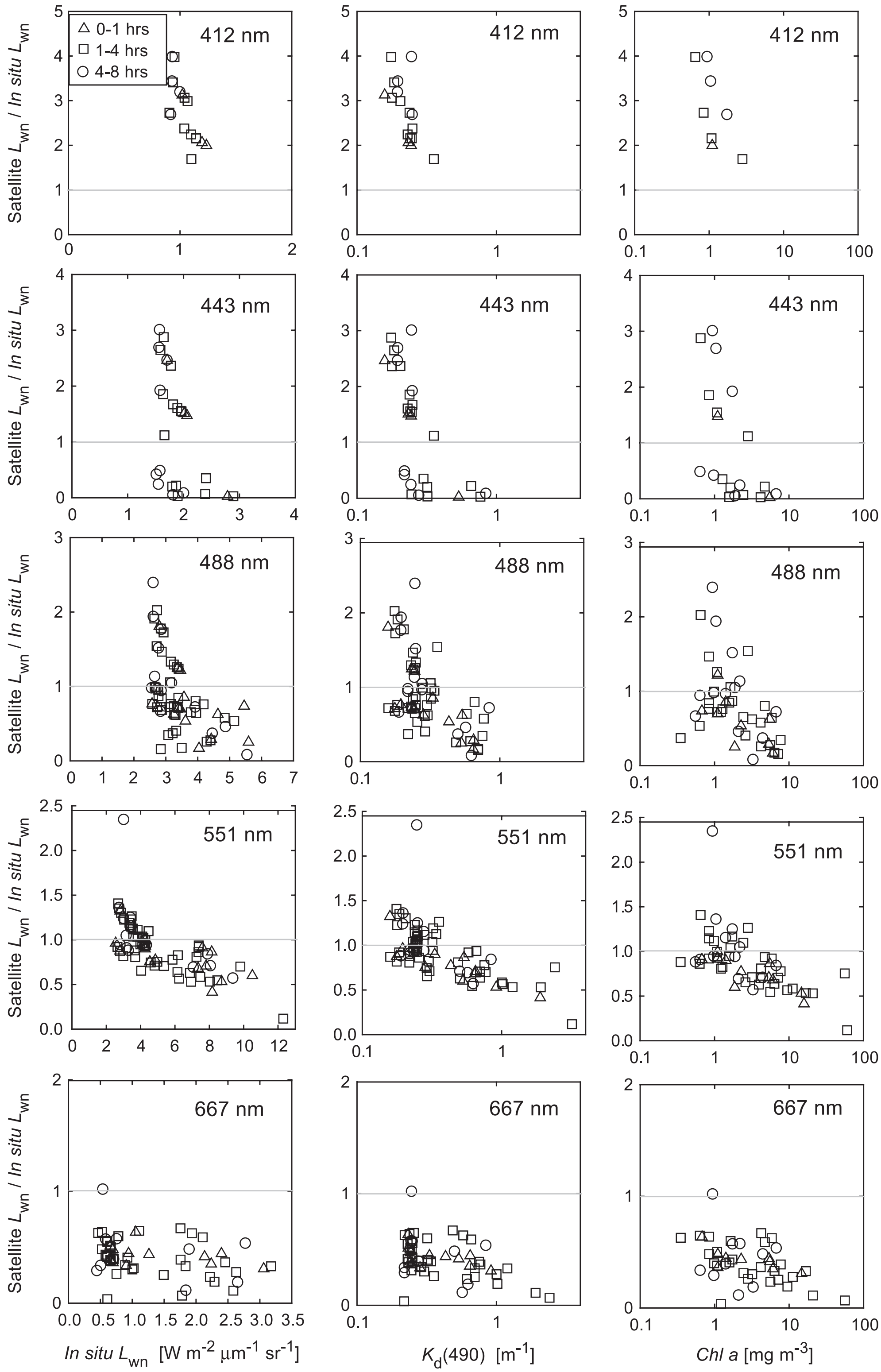

Fig. 18. The ratio of satellite-derived normalized water-leaving radiance from MODIS imagery to measured in situ normalized water-leaving radiance at different light wavelengths as indicated in each graph. This ratio is plotted as a function of three parameters: first, in situ normalized water-leaving radiance (graphs in the left-hand column); second, diffuse attenuation coefficient for downwelling irradiance at $\lambda = 490$ nm (graphs in the middle column), and third, chlorophyll *a* concentration (graphs in the right-hand column). The horizontal line in each graph corresponds to the perfect agreement between the match-up data of satellite-derived L_{wn} and in situ L_{wn}. The use of symbols for data points as in Fig. 16.

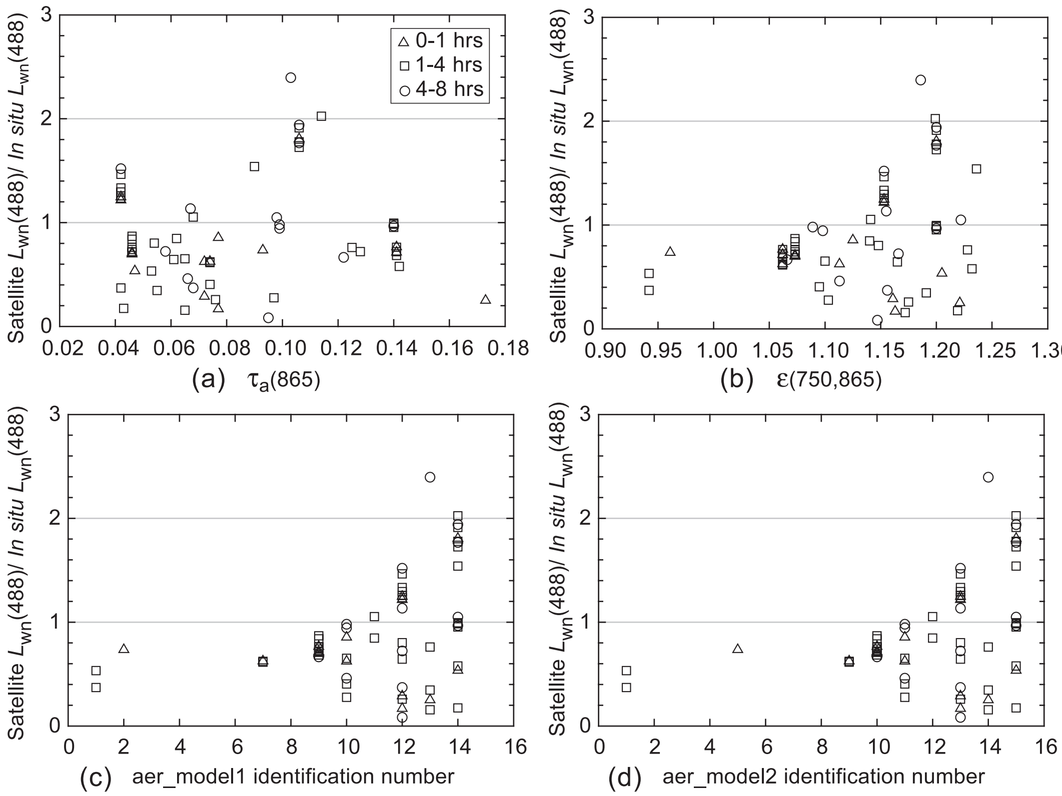

Fig. 19. The ratio of satellite-derived normalized water-leaving radiance from MODIS imagery to measured in situ normalized water-leaving radiance at light wavelength of 488 nm. This ratio is plotted in four graphs as a function of (a) MODIS-derived aerosol optical thickness at 865 nm, $\tau_a(865)$, (b) atmospheric-correction parameter $\varepsilon(750,865)$, (c) aerosol model identification number from the first group of models, aer_model1, and (d) aerosol model identification number from the second group of models, aer_model2. The use of symbols for data points as in Fig. 16.

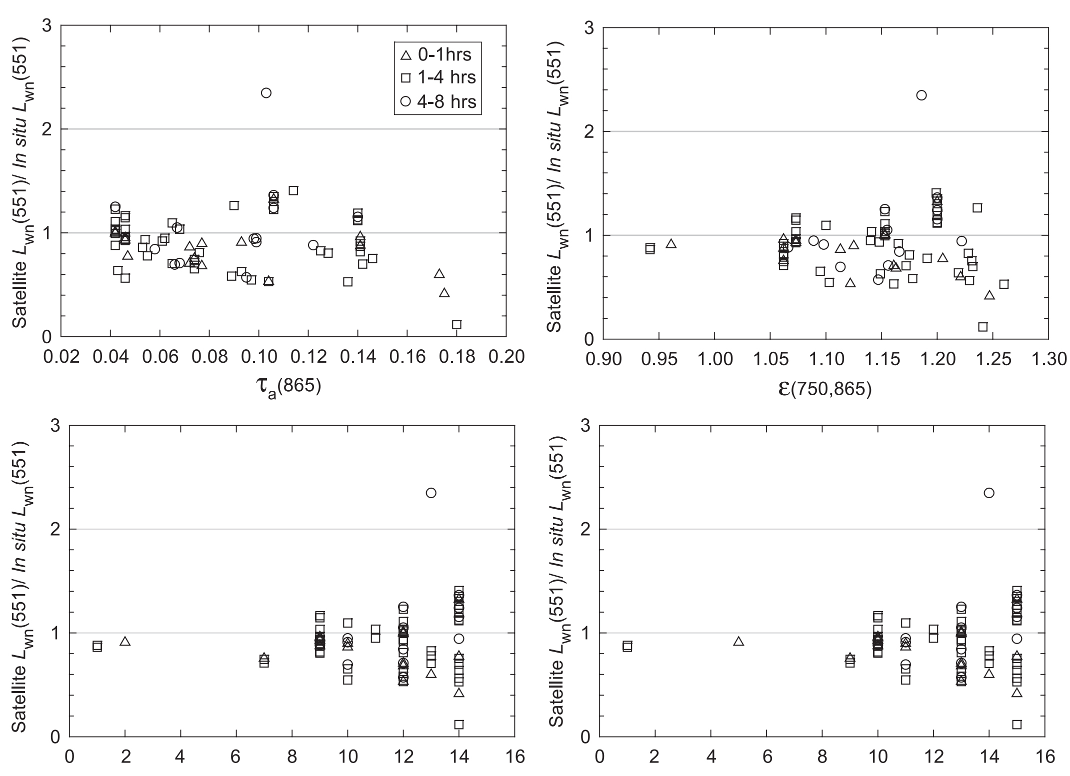

Fig. 20. As Fig. 19, but for the ratio of normalized water-leaving radiance at 551 nm.

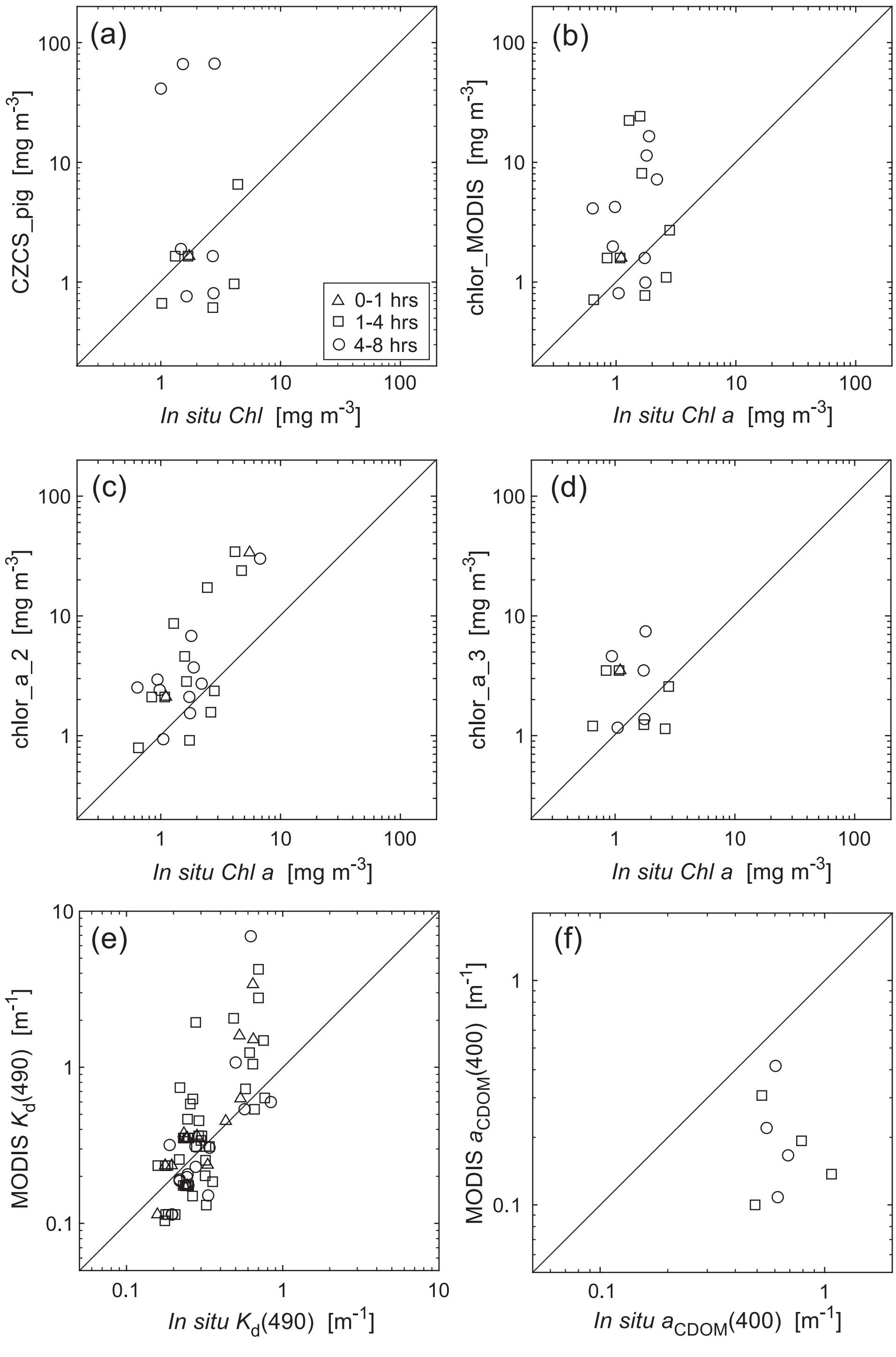

Fig. 21. Comparisons of satellite-derived bio-optical data products obtained from MODIS imagery using standard MODIS algorithms with sea truth data obtained from our field measurements. (a) MODIS-derived chlorophyll (plus phaeopigments) concentration from CZCS_pigm algorithm vs. chlorophyll concentration measured on surface water samples, (b) MODIS-derived chlorophyll *a* concentration from chlor_MODIS algorithm vs. measured chlorophyll *a* concentration, (c) MODIS-derived chlorophyll *a* concentration from chlor_a_2 algorithm vs. measured chlorophyll *a* concentration, (d) MODIS-derived chlorophyll *a* concentration from chlor_a_3 algorithm vs. measured chlorophyll *a* concentration, (e) MODIS-derived diffuse attenuation coefficient of downwelling irradiance at 490 nm from MODIS K_490 algorithm vs. measured coefficient $K_d(490)$, (f) MODIS-derived CDOM absorption coefficient at 400 nm vs. measured coefficient $a_{CDOM}(400)$.

near-infrared part of the spectrum are negligible (i.e., for the 750- and 865-nm MODIS bands, and 765- and 865-nm SeaWiFS bands). However, this assumption is not valid over turbid waters due to significant light scattering by suspended particles and in shallow waters due to bottom reflectance. By comparing nearly simultaneous match-ups

Table 7
Summary of the error analysis based on match-up comparisons between the MODIS-derived L_{wn} and sea truth L_{wn} data

L_{wn}	MNB (%)	RMS (%)	log_bias	log_rms	*n*
nLw qual = 0					
412 nm	178	69	0.43	0.11	17
443 nm	28	105	− 0.22	0.71	29
488 nm	− 11	50	− 0.13	0.28	70
551 nm	− 13	33	− 0.10	0.21	85
667 nm	− 59	18	− 0.46	0.34	59

nLw qual = 0 indicates that only the highest quality satellite L_{wn} data (i.e., with a quality level 0) were used in this comparison.

of SeaWiFS and field observations of water-leaving reflectance, Siegel et al. (2000) showed that the inappropriate application of the black pixel assumption is, at least partly, responsible for significant overcorrection of atmospheric effects in productive waters with higher chlorophyll concentration (>2 mg m^{-3}). They showed that the overcorrection is most pronounced in the violet and blue spectral region and increases dramatically with an increase in chlorophyll concentrations beyond the value of 2 mg m^{-3}. Our results from the Baltic Sea at the waveband of 551 nm appear to be consistent with such dependence of overcorrection on Chl *a* (Fig. 18). However, in the red band of 667 nm, the overcorrection is observed over the entire range of Chl *a* in our data set, including relatively low concentrations of < 1 mg m^{-3}. At the violet band of 412 nm, we have only a few match-up points that were all collected at relatively low Chl *a* of < 3 mg m^{-3}. They all show an undercorrection of atmospheric effects resulting in the overestimation of satellite-derived $L_{wn}(412)$. In the blue bands of 443 and 488 nm, there is a clear tendency for overcorrection of atmospheric effects at high Chl *a*, but at lower Chl *a*, our data include both the significant undercorrection and overcorrection.

The match-up comparisons in Fig. 18 suggest that in addition to the black pixel assumption, there are certainly other factors in the atmospheric correction procedure which affect satellite retrievals of L_{wn}. The modeling treatment of aerosols is usually considered an important potential source of error in the atmospheric correction. Figs. 19 and 20 show the ratio of satellite-derived to in situ-derived L_{wn} for 488 and 551 nm respectively, as a function of aerosol-related parameters that are crucial to the atmospheric correction procedure. These parameters include the MODIS-derived aerosol optical thickness at 865 nm, $\tau_a(865)$ (MODIS product denoted as Tau_865), the MODIS-derived atmospheric-correction parameter $\varepsilon(750,865)$ (MODIS product Eps_78), and the various types of aerosol models identified by sequential numbers from 1 to 14 or 15. The parameter $\varepsilon(750,865)$ is essential for selecting an appropriate aerosol model from all candidate models, which then allows a determination of wavelength-dependent multiple scattering effects associated with aerosols in the atmospheric correction procedure (Gordon, 1997; Gordon & Voss, 1999; Gordon & Wang, 1994). The two groups of aerosol models referred to as aer_model1 and aer_model2 include models producing two values of $\varepsilon(750,865)$ that bracket the satellite-derived $\varepsilon(750,865)$.

For our match-up data set, the aerosol optical thickness $\tau_a(865)$ varied over a fairly broad range from about 0.04 to 0.18 (Figs. 19 and 20). The two L_{wn} ratios, i.e., satellite $L_{wn}(488)$/in situ $L_{wn}(488)$ and satellite $L_{wn}(551)$/in situ $L_{wn}(551)$, show no apparent relationship with $\tau_a(865)$, perhaps with the exception that the satellite L_{wn} values are clearly underestimated at the highest values of $\tau_a(865)$. The MODIS-derived $\varepsilon(750,865)$ parameter varied between 0.95 and 1.25 and shows no relationship with the L_{wn} ratios considered. The errors in retrievals of $L_{wn}(488)$ and $L_{wn}(551)$ do not seem to be related to the type of aerosol model selected in the atmospheric correction procedure either. We see that the models with a high identification number (>10) from both the aer_model1 group and the aer_model2 group, result in underestimates and overestimates of $L_{wn}(488)$ and $L_{wn}(551)$. One possible trend with regard to the type of aerosol model is the underestimation of $L_{wn}(488)$ by models that are identified by low numbers (1 and 2), but very few data for these cases limit the significance of this observation. The most important conclusion from this analysis is that the application of the current standard atmospheric correction procedure in the Baltic will produce, with relatively high probability, unacceptably large errors in retrievals of water-leaving radiances from the MODIS sensor. In order to achieve significant improvements, it seems necessary to develop and apply specialized aerosol models and new algorithmic approaches based on methods appropriate for Case 2 waters or turbid coastal/inland waters (e.g., Hu et al., 2000; Land & Haigh, 1996; Ruddick et al., 2000).

Because both the standard atmospheric correction procedure and standard bio-optical in-water algorithms that are applied to MODIS/Terra imagery have been shown to produce large discrepancies in comparison with sea truth data, we expect that the match-up comparisons of nearly

Table 8
Summary of the error analysis based on match-up comparisons between the MODIS-derived bio-optical data products and sea truth data

	MNB (%)	RMS (%)	log_bias	log_rms	*n*
CZCS_pigm					
Chl(spectrophotometric)	730	1556	0.17	0.78	14
chlor_MODIS					
Chl *a*(spectrophotometric)	388	584	0.40	0.53	20
Chl *a*(HPLC)	467	888	0.39	0.58	20
chlor_a_2					
Chl *a*(spectrophotometric)	208	227	0.36	0.35	25
Chl *a*(HPLC)	270	353	0.37	0.44	25
chlor_a_3					
Chl *a*(spectrophotometric)	129	157	0.24	0.35	12
Chl *a*(HPLC)	133	180	0.21	0.41	12
absorp_coeff_gelb	− 69	21	− 0.62	0.33	9
K_490	57	162	0.08	0.28	77

simultaneous satellite and field determinations of bio-optical properties of the Baltic waters will also show large discrepancies. Such match-up comparisons are shown for four pigment data products, CZCS_pigm, chlor_MODIS, chlor_a_2, and chlor_a_3, as well as for the diffuse attenuation coefficient at 490 nm and CDOM absorption coefficient at 400 nm (Fig. 21). As expected, the differences between the satellite-derived data and in situ match-ups are usually large. The statistical errors for these data are summarized in Table 8.

The standard atmospheric correction procedure for MODIS is very similar to that for the SeaWiFS sensor (Gordon, 1997), although some differences result from the fact that these sensors have spectral bands centered at somewhat different wavelengths, for example, the near-infrared MODIS band is at 750 nm and SeaWiFS band is at 765 nm. The same set of our sea truth L_{wn} measurements in the Baltic was used again for the comparisons with SeaWiFS-derived L_{wn}. The only difference in these match-up data sets is that the MODIS overpasses above the site of field measurements occurred earlier during the day than the SeaWiFS overpasses (the time differences between the MODIS and SeaWiFS overpasses were from about 15 min to 2 h). For every day with good-quality MODIS data, there were also available SeaWiFS data that were used for match-up comparisons shown in Fig. 22. These comparisons show that retrievals of L_{wn} from SeaWiFS imagery in the Baltic frequently provide significantly lower values compared to our in situ measurements. In fact, the SeaWiFS data processing often returns negative values of L_{wn}, especially in the violet and blue spectral channels. The poor agreement between the satellite and in situ values of L_{wn} appears in our match-up data set regardless of whether the data were collected in winter, spring, summer or autumn, and also regardless of whether the data were collected in the Gulf of Gdansk, Pomerania Bay, along the Polish coast, or in the central Baltic.

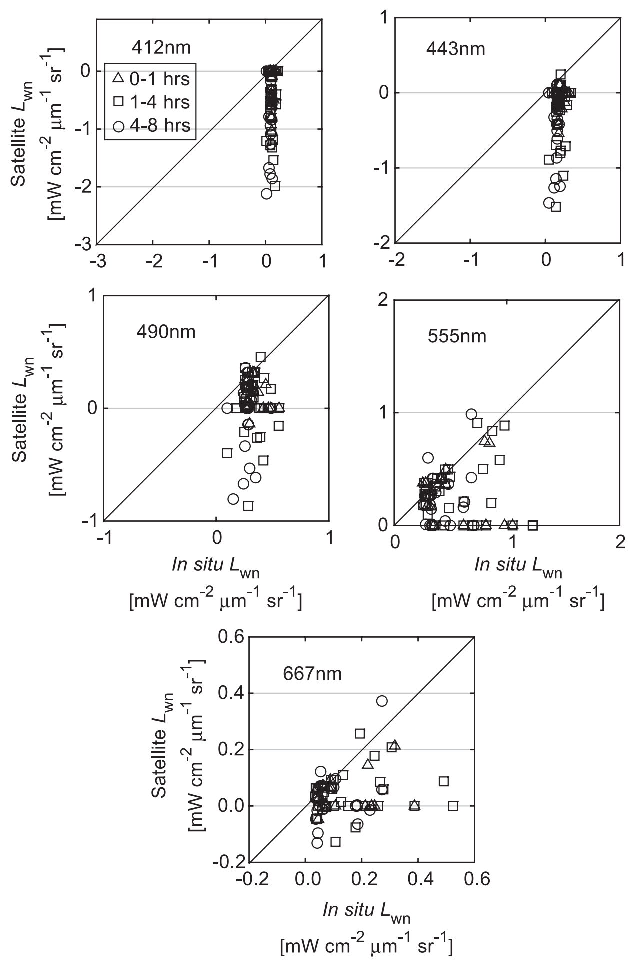

Fig. 22. Comparisons of match-up data of normalized water-leaving radiance measured in situ and derived from SeaWiFS satellite imagery for spectral bands centered at 412, 443, 490, 555, and 667 nm. As indicated, the triangles represent match-up data with the time shift no greater than 1 h between the satellite overpass and in situ measurement, the squares correspond to the time shift of 1–4 h, and the circles to the time shift of 4–8 h. The line represents the one-to-one perfect agreement.

6. Conclusions

We tested the performance of the MODIS operational algorithms for retrieving pigments, $K_d(490)$, and $a_{CDOM}(400)$, and the SeaWiFS OC4v4 algorithm for retrieving chlorophyll *a* using an extensive bio-optical data set collected on 25 cruises between 1993 and 2001 in the Baltic Sea. Our analysis revealed a systematic and large overestimation of chlorophyll products for the MODIS and SeaWiFS algorithms. This result includes the semianalytical algorithm based on the model of Carder et al. (1999) which was designed to have an improved performance in Case 2 waters. It appears that the Baltic waters require new approaches and new parameterizations for both empirical and semianalytical pigment algorithms. We tested the extent of improvements that can be achieved with minor alterations to the present standard algorithms. By keeping the equations of the algorithms essentially unchanged, we determined new coefficients for the algorithms using our database from field measurements. The bias of the retrieved data products from such regionally tuned standard algorithms was significantly reduced. The regional MODIS chlor_a_2 algorithm performed slightly better than other pigment algorithms. The mean normalized bias (MNB) for the Baltic_chlor_a_2 algorithm was reduced to 26% (from over 200% for the standard chlor_a_2 algorithm), but the root mean square (RMS) error still remained large (>100%). Thus, the standard pigment algorithms, even with region-specific parameterizations, will have inadequate accuracy. By far, the best results were obtained by applying the Baltic-specific parameterization to the MODIS K_490 algorithm for estimating the diffuse attenuation coefficient of downwelling irradiance, $K_d(490)$. For this regional version of the $K_d(490)$ algorithm, the MNB and RMS errors were reduced to 4% and 30%, respectively.

Inadequate in-water bio-optical algorithms are one possible source of error in satellite-derived ocean color data products. Another source of error is associated with the atmospheric correction procedure, in which the water-leaving radiance is retrieved from radiance measured by a satellite sensor by subtracting the effects due to atmosphere and sea surface. Part of our database from measurements in the Baltic was used for direct comparisons with satellite-derived water-leaving radiances and other satellite-derived data products. Although our match-up data set is limited in its size, it is sufficient to reveal a consistently poor agreement between in situ-measured water-leaving radiances, $L_{wn}(\lambda)$, and satellite-derived $L_{wn}(\lambda)$ from the MODIS/Terra and SeaWiFS sensors. Assuming that the in situ determinations are reasonably accurate, these match-up comparisons indicate that the current atmospheric correction for MODIS and SeaWiFS usually fails to retrieve $L_{wn}(\lambda)$ in the Baltic. This problem is especially well pronounced in the blue spectral bands (412, 443, and 488 nm) where we observed no covariation between in situ and satellite values of $L_{wn}(\lambda)$.

Acknowledgements

This research was supported by the Polish National Committee for Scientific Research—Grant PBZ-KBN 056/P04/2001. Partial support was provided by the NASA EOS Validation Grant NAG5-6466 to D. Stramski. We wish to thank all the colleagues who participated in the Baltic cruises as well as the officers and crews of the R/V *Oceania* for assistance in the collection of field data and logistical support. Special thanks are due to A. Ston, S. Kaczmarek, and P. Kowalczuk for making available the chlorophyll and CDOM data, R. Evans and W. Baringer for processing and providing MODIS data, K. Carder and R. Chen for computer code of the semianalytical algorithm, K. Kilpatrick for an update of the MODIS algorithm coefficients, and D. Clark for useful discussion.

Appendix A

Standard MODIS and SeaWiFS in-water bio-optical algorithms examined in this study

---

TERRA/MODIS product number MOD 19, parameter number 13
CZCS total pigment concentration – CZCS_pigm
(Clark, 1997; K. Kilpatrick, private communication, April 2002).

$$\mathrm{CZCS\_pigm} = 10^{(aX^3+bX^2+cX+d)/e}$$

$X = \log_{10}[L_{wn}(443)/L_{wn}(551)]$
where the coefficients for the high X are:
$a = -1.4443$, $b = 1.4947$, $c = -1.5283$, $d = -0.0433$, and $e = 1$,
and for the low X:
$a = -5.0511$, $b = 2.8952$, $c = -0.5069$, $d = -0.1126$, and $e = 1$,
and the switch point between the low and high X is 0.7368

TERRA/MODIS product number MOD 19, parameter number 14
Chlorophyll *a* concentration for Case 1 water – chlor_MODIS
(Clark, 1997; K. Kilpatrick, private communication, April 2002).

$$\mathrm{chlor\_MODIS} = 10^{(aX^3+bX^2+cX+d)/e}$$

$X = \log_{10}\{[L_{wn}(443) + L_{wn}(488)]/L_{wn}(551)\}$
where the coefficients for the high X are:
$a = -2.8237$, $b = 4.7122$, $c = -3.9110$, $d = 0.8904$, and $e = 1$,
and for the low X:
$a = -8.1067$, $b = 12.0707$, $c = -6.0171$, $d = 0.8791$, and $e = 1$,
and the switch point between the low and high X is 0.9866

TERRA/MODIS product number MOD 26, parameter number 23
Diffuse attenuation coefficient for downwelling irradiance at 490 nm – K_490
(Clark, 1997; K. Kilpatrick, private communication, April 2002).

$$\mathrm{K\_490} = 0.016 + 0.156445X^{-1.5401}$$

where $X = L_{wn}(488)/L_{wn}(551)$

TERRA/MODIS product number MOD 21, parameter number 26
Chlorophyll *a* concentration for Case 2 water (SeaWiFS OC3M) – chlor_a_2
(O'Reilly et al., 2000).

$$\mathrm{chlor\_a\_2} = 10^{(0.2830-2.753X+1.457X^2+0.659X^3-1.403X^4)}$$

$X = \log_{10}[\max(r_{25}, r_{35})]$ where $r_{25} = R_{rs}(443)/R_{rs}(551)$, $r_{35} = R_{rs}(488)/R_{rs}(551)$

TERRA/MODIS product number MOD 21, parameter number 27
Chlorophyll *a* concentration for Case 2 water – chlor_a_3
(Carder et al., 1999; see also Carder et al., 2003).

The computer code of the full semianalytical algorithm was received from K. Carder and R. Chen in April 2002.

For default cases, the chlorophyll *a* concentration was calculated from empirical algorithms:

$$\mathrm{chlor\_a\_3} = 10^{(0.289-3.20X+1.2X^2)}$$

where $X = \log_{10}[R_{rs}(488)/R_{rs}(551)]$

The phytoplankton absorption coefficient at 675 nm, a_{Φ} (675 nm), and CDOM absorption at 400 nm, a_{CDOM}(400 nm) (or absorp_coeff_gelb), for default cases were calculated from:

$$a_{\Phi}(675) = 0.328[10^{-0.919+1.037r_{25}-0.407r_{25}^2-3.531r_{35}+1.702r_{35}^2} - 0.008]$$

$$a_{CDOM}(400) = 1.5[10^{-1.147+1.963r_{15}-1.01r_{15}^2-0.856r_{25}+1.702r_{25}^2}]$$

where:
$r_{15} = \log[R_{rs}(412)/R_{rs}(551)]$, $r_{25} = \log[R_{rs}(443)/R_{rs}(551)]$, and
$r_{35} = \log[R_{rs}(488)/R_{rs}(551)]$

SeaWiFS OC4v4 algorithm
Chlorophyll *a* concentration – chlor_OC4v4
(O'Reilly et al., 2000).

$$\mathrm{chlor\_OC4v4} = 10^{(0.366-3.067X+1.930X^2+0.649X^3-1.532X^4)}$$

$X = \log_{10}\{\max[R_{rs}(443)/R_{rs}(555), R_{rs}(490)/R_{rs}(555), R_{rs}(510)/R_{rs}(555)]\}$

References

Bukata, R. P., Jerome, J. H., Kondratyev, K. Ya., & Pozdnyakov, D. V. (1995). *Optical properties and remote sensing of inland and coastal waters*. Boca Raton: CRC Press.

Carder, K. L., Chen, F. R., Lee, Z. P., & Hawes, S. K. (1999). Semianalytic moderate-resolution imaging spectrometer algorithms for chlorophyll *a* and absorption with bio-optical domains based on nitrate-depletion temperatures. *Journal of Geophysical Research*, *104*, 5403–5421.

Carder, K. L., Chen, F. R., Lee, Z., Hawes, S. K., & Cannizzaro, J. P. (2003). MODIS Ocean Science Team Algorithm Theoretical Basis Document, ATBD 19, Case 2 Chlorophyll *a*, version 7, http://modis.gsfc.nasa.gov/data/atbd/atbd_mod19.pdf.

Clark, D. K. (1997). *MODIS Algorithm Theoretical Basis Document, Bio-Optical Algorithms—Case 1 Waters*, version 1.2, http://modis.gsfc.nasa.gov/data/atbd/atbd_mod18.pdf.

Clarke, G. L., Ewing, G. C., & Lorenzen, C. J. (1970). Spectra of back-scattered light from the sea obtained from aircraft as a measure of chlorophyll concentration. *Science*, *167*, 1119–1121.

Darecki, M., Weeks, A., Sagan, S., Kowalczuk, P., & Kaczmarek, S. (2003). Optical characteristics of two contrasting Case 2 waters and their influence on remote sensing algorithms. *Continental Shelf Research*, *23*, 237–250.

Esaias, W. E., Abbott, M. R., Barton, I., Brown, O. B., Campbell, J. W., Carder, K. L., Clark, D. K., Evans, R. H., Hoge, F. E., Gordon, H. R., Balch, W. M., Letelier, R., & Minnett, P. J. (1998). An overview of MODIS capabilities for ocean science observations. *IEEE Transactions on Geoscience and Remote Sensing*, *36*, 1250–1265.

Evans, R. H., & Gordon, H. R. (1994). CZCS system calibration: A retrospective examination. *Journal of Geophysical Research*, *99*, 7293–7307.

Gordon, H. R. (1997). Atmospheric correction of ocean color imagery in the Earth Observing System era. *Journal of Geophysical Research*, *102*, 17081–17106.

Gordon, H. R., Clark, D. K., Mueller, J. L., & Hovis, W. A. (1980). Phytoplankton pigments from the Nimbus-7 Coastal Zone Color Scanner: Comparisons with surface measurements. *Science*, *210*, 63–66.

Gordon, H. R., & Ding, K. (1992). Self-shading of in-water instruments. *Limnology and Oceanography*, *37*(3), 491–500.

Gordon, H. R., & Morel, A. (1983). Remote assessment of ocean color for interpretation of satellite visible imagery—A review. In R. T. Barber, M. J. Bowman, C. N. K. Mooers, & B. Zetzschel (Eds.), *Lecture notes on coastal and estuarine studies* (pp. 1–144). New York: Springer-Verlag.

Gordon, H. R. & Voss, K. J. (1999). *MODIS Normalized Water-leaving Radiance, Algorithm Theoretical Basis Document (MOD 18)*, version 4, http://modis.gsfc.nasa.gov/data/atbd/ atbd_mod17.pdf.

Gordon, H. R., & Wang, M. (1994). Retrieval of water-leaving radiance and aerosol optical thickness over the oceans with SeaWiFS: A preliminary algorithm. *Applied Optics*, *33*, 443–452.

HELCOM (1988). *Guidelines for Baltic Monitoring Program*. Helsinki: Baltic Marine Environment Protection Commission, 116 pp.

Hooker, S. B., & McClain, C. R. (2000). The calibration and validation of SeaWiFS data. *Progress in Oceanography*, *45*, 427–465.

Hovis, W. A., Clark, D. K., Austin, R. W., Wilson, W. H., Baker, E. T., Ball, D., Gordon, H. R., Mueller, J. L., El-Sayed, S. Z., Sturm, B., Wrigley, R. C., & Yentsch, C. S. (1980). Nimbus-7 Coastal Zone Color Scanner: System description and initial imagery. *Science*, *210*, 60–63.

Højerslev, N. K., & Aas, E. (2001). Spectral light absorption by yellow substance in the Kattegat–Skagerrak area. *Oceanologia*, *43*, 39–60.

Hu, C., Carder, K. L., & Muller-Karger, F. E. (2000). Atmospheric correction of SeaWiFS imagery over turbid coastal waters: A practical method. *Remote Sensing of Environment*, *74*, 195–206.

Kowalczuk, P. (1999). Seasonal variability of yellow substance absorption in the surface layer of the Baltic Sea. *Journal of Geophysical Research*, *104*, 30047–30058.

Kowalczuk, P., & Darecki, M. (1998, 10–13 November). The relative share of light absorption by yellow substances in total light absorption in the surface layer of southern Baltic sea. In S. G. Ackleson (Ed.), *Proceedings of Ocean Optics XIV Conference, Kailua Kona, Hawaii, USA, vol. 1052*, 9 pp. CD-ROM.

Land, P. E., & Haigh, J. D. (1996). Atmospheric correction over case 2 waters with an interactive fitting algorithm. *Applied Optics*, *35*, 5443–5451.

Loisel, H., & Stramski, D. (2000). Estimation of the inherent optical properties of natural waters from irradiance attenuation coefficient and reflectance in the presence of Raman scattering. *Applied Optics*, *39*, 3001–3011.

Loisel, H., Stramski, D., Mitchell, B. G., Fell, F., Fournier-Sicre, V., Lamasle, B., & Babin, M. (2001). Comparison of the ocean inherent optical properties obtained from measurements and inverse modeling. *Applied Optics*, *40*, 2384–2397.

Mitchell, B. G., Bricaud, A., Carder, K., Cleveland, J., Ferrari, G., Gould, R., Kahru, M., Kishino, M., Maske, H., Moisan, T., Moore, L., Nelson, N., Phinney, D., Reynolds, R., Sosik, H., Stramski, D., Tassan, S., Trees, C., Weidemann, A., Wieland, J., & Vodacek, A. (2000). Determination of spectral absorption coefficients of particles, dissolved material and phytoplankton for discrete water samples. In G. S. Fargion, & J. L. Mueller (Eds.), *Ocean optics protocols for satellite ocean color sensor validation. Revision 2. NASA Technical Memorandum, 2000-209966* (pp. 125–153). Maryland: NASA Goddard Space Center Greenbelt.

Mitchell, B. G., Kahru, M., Wieland, J., & Stramska, M. (2002). Determination of spectral absorption coefficients of particles, dissolved material and phytoplankton for discrete water samples. In J. L. Mueller, & G. S. Fargion (Eds.), *Ocean optics protocols for satellite ocean color sensor validation. Revision 3, NASA Technical Memorandum, 2002-21004/Rev3, vol. 2* (pp. 231–257). Maryland: NASA Goddard Space Center Greenbelt.

Morel, A. (1998). Minimum requirements for an operational ocean-colour sensor for the open ocean. *IOCCG Report, vol. 1*. Dartmouth, Nova Scotia: IOCCG Project Office, 46 pp.

Morel, A., & Prieur, L. (1977). Analysis of variations in ocean colour. *Limnology and Oceanography*, *22*, 709–722.

Mueller, J. L., & Austin, R. W. (1995). In S. B. Hooker, E. R. Firestone, & J. G. Acker (Eds.), *Ocean optics protocols for SeaWiFS validation, Revision 1NASA Technical Memorandum 104566, vol. 25*. Greenbelt, MD: NASA Goddard Space Center, 67 pp.

O'Reilly, J. E., Maritorena, S., Mitchell, B. G., Siegel, D. A., Carder, K. L., Garver, S. A., Kahru, M., & Mcclain, C. (1998). Ocean color chlorophyll algorithms for SeaWiFS. *Journal of Geophysical Research*, *103*, 24937–24953.

O'Reilly, J. E., Maritorena, S., Siegel, D. A., O'Brien, M. C., Toole, D., Mitchell, B. G., Kahru, M., Chavez, F. P., Strutton, P., Cota, G. F., Hooker, S. B., McClain, C. R., Carder, K. L., Müller-Karger, F., Harding, L., Magnuson, A., Phinney, D., Moore, G. F., Aiken, J., Arrigo, K. R., Letelier, R., & Culver, M. (2000). Ocean color chlorophyll algorithms for SeaWiFS, OC2, and OC4: Version 4. In S. B. Hooker, & E. R. Firestone (Eds.), *SeaWiFS Postlaunch Calibration and Validation Analyses, Part 3, NASA Technical Memorandum, 2000-206892, vol. 11* (pp. 9–27). Greenbelt, MD: NASA Goddard Space Center.

Ruddick, K. G., Ovidio, F., & Rijkeboer, M. (2000). Atmospheric correction of SeaWiFS imagery for turbid coastal and inland waters. *Applied Optics*, *39*, 897–912.

Sathyendranath, S. (Ed.) (2000). *Remote sensing of ocean colour in coastal, and other optically-complex, watersIOCCG Report, vol. 3*. Dartmouth, Nova Scotia: IOCCG Project Office, 140 pp.

Schotz, F. (1962). Pigmentanalytische untersuchungen an Oenothera.I.Vorversuche und analyse der blatter und bluten von Oenothera suaveolens Desf., Mutante 'wiesshers'. *Planta*, *58*, 411–434.

Siegel, D. A., & Michaels, A. F. (1996). Quantification of non-algal light attenuation in the Sargasso Sea: Implication for biogeochemistry and remote sensing. *Deep-Sea Research II*, *43*, 321–345.

Siegel, D. A., Wang, M., Maritorena, S., & Robinson, W. (2000). Atmospheric correction of satellite ocean color imagery: The black pixel assumption. *Applied Optics*, *39*, 3582–3591.

Stramski, D., & Tegowski, J. (2001). Effects of intermittent entrainment of air bubbles by breaking wind waves on ocean reflectance and underwater light field. *Journal of Geophysical Research*, *106*, 31345–31360.

Terrill, E. J., Melville, W. K., & Stramski, D. (2001). Bubble entrainment by breaking waves and their influence on optical scattering in the upper ocean. *Journal of Geophysical Research*, *106*, 16815–16823.

Yan, B., Stamnes, K., Li, W., Chen, B., Stamnes, J. J., & Tsay, S. -C. (2002). Pitfalls in atmospheric correction of ocean color imagery: How should aerosol optical properties be computed? *Applied Optics*, *41*, 412–423.

Zibordi, G., & Ferrari, G. M. (1995). Instrument self-shading in underwater optical measurements: Experimental data. *Applied Optics*, *34*(2), 2750–2754.